CHEMISTRY
A EUROPEAN JOURNAL

DOI: 10.1002/chem.200501011

Spatial Extent of the Singlet and Triplet Excitons in Luminescent Angular-Shaped Transition-Metal Diynes and Polyynes Comprising Non-π-Conjugated Group 16 Main Group Elements

Suk-Yue Poon,[a] Wai-Yeung Wong,*[a] Kok-Wai Cheah,[b] and Jian-Xin Shi[a]

Abstract: A novel approach based on conjugation interruption has been developed and is presented for a series of luminescent and thermally stable chalcogen-bridged platinum(II) polyyne polymers *trans*-[{−Pt(PBu_3)$_2$C≡C-(C_6H_4)E(C_6H_4)C≡C−}$_n$] (E = O, S, SO, SO_2). Particular attention was focused on the photophysical properties of these Group 10 polymetallaynes and comparison was made to their binuclear model complexes *trans*-[Pt(Ph)-(PEt_3)$_2$C≡C(C_6H_4)E(C_6H_4)C≡CPt(Ph)-(PEt_3)$_2$] and their closest Group 11 gold(I) and Group 12 mercury(II) neighbours, [MC≡C(C_6H_4)E(C_6H_4)C≡CM] (M = Au(PPh_3), HgMe; E = O, S, SO, SO_2). The regiochemical structures of these angular-shaped molecules were studied by NMR spectroscopy and single-crystal X-ray structural analyses. Upon photoexcitation, each one has an intense purple-blue fluorescence emission near 400 nm in dilute fluid solutions at room temperature. Harvesting of the organic triplet emissions harnessed through the strong heavy-atom effects of Group 10–12 transition metals was studied in detail. These metal-containing aryleneethynylenes spaced by chalcogen units were found to have large optical gaps and high-energy triplet states. The influence of metal- and chalcogen-based conjugation interrupters on the intersystem crossing rate and on the spatial extent of the lowest singlet and triplet excitons was fully elucidated. We discuss and compare the phosphorescence spectra of these transition-metal diynes and polyynes in terms of the nature of the metal centre, conjugated chain length and Group 16 spacer unit. Our work here indicates that high-energy triplet states in these materials intrinsically give rise to very efficient phosphorescence with fast radiative decays and one could readily observe room-temperature phosphorescence for the platinum polyynes.

Keywords: alkynes · chalcogens · gold · mercury · phosphorescence · platinum

Introduction

Over the past decade, conjugated ethynylated materials, such as arylacetylenes,[1–4] polyarylenethynylenes[5,6] and metal-containing acetylide complexes and polymers,[7,8] have become the subject of numerous research endeavours, leading to a number of significant technological developments within the realm of molecular electronics and materials science. The use of platinium-containing polyynes both as semiconductors and triplet emitters has been proposed.[7,8] While considerable work has been devoted to investigations of the nature of singlet excited states in conjugated polymers,[9–11] much less is known about the nature of their triplet excited states. It was shown that the triplet states play an increasing vital role in the ultimate efficiency of light-emitting diodes (LEDs). For example, photoluminescence is affected by the relative energies of the singlet and triplet states, and the overall efficiency of LEDs is controlled by the fraction of triplet states generated or harvested.[12–15] To better understand the role of triplet states in optical and electrical processes within conjugated materials and their potential for a number of applications,[16–22] a comprehensive investigation of their photophysics is essential. In the literature, work on the nonradiative decay of triplet states in conjugated polymers is still in its infancy. Yet radiationless transitions are more common than radiative transitions, so a

[a] S.-Y. Poon, Dr. W.-Y. Wong, Dr. J.-X. Shi
Department of Chemistry and Centre for Advanced Luminescence Materials
Hong Kong Baptist University
Waterloo Road, Kowloon Tong, Hong Kong (P. R. China)
Fax: (+852) 3411-7348
E-mail: rwywong@hkbu.edu.hk

[b] Prof. K.-W. Cheah
Department of Physics and Centre for Advanced Luminescence Materials
Hong Kong Baptist University
Waterloo Road, Kowloon Tong, Hong Kong (P. R. China)

knowledge of triplet-state-decay mechanisms is necessary for a full understanding of the photochemistry of conjugated arylene–ethynylene systems.

We and others have circumvented the problem of the triplet state being nonemissive by using a model system consisting of d^8 Pt-containing ethynylenic conjugated complexes and polymers of the general form *trans*-[{−Pt(PBu_3)$_2$C≡CRC≡C−}$_n$] for which phosphorescence can be observed and the triplet energies can be estimated directly.[7,23,24] The triplet energy level can be tuned over a wide range by varying the spacer group R. This has enabled a detailed study of the relationship between triplet energy and the rate of nonradiative decay for this class of conjugated materials. More recently, similar research work has been extended to their closest neighbours, such as d^{10} gold(I)[25] and mercury(II) complexes.[26] When a heavy atom is introduced into the main chain, the intersystem crossing (ISC) rate is increased due to the enhanced spin–orbit coupling. A number of literature reports have shown that the nonradiative decay of the triplet states in a series of platinum-containing conjugated polymers and their metal model complexes can be described well by the energy-gap law[23a] and, therefore, work should focus on materials with high-energy triplets to avoid competition with nonradiative decay. In contrast to the body of work on luminescent metallaynes with the π-electron conjugated unit, there are no reports of similar systems possessing Group 16 chalcogen units in the backbone. There are also numerous reports on the syntheses and applications of purely organic polymeric systems of arylene ether, sulfide, sulfoxide and sulfone in the literature,[27–30] but little research on rigid-rod chalcogen-derived metallaynes and their corresponding polyynes has been carried out. To get a deeper insight, it is important to develop synthetic strategies leading to novel conjugated polymers with non-π-conjugated Group 16 heteroatoms in the polymer chains. While the heteroatom can act as the conjugation-breaking unit to interrupt the electronic π conjugation, these materials can also offer an attractive combination of physical, optical and mechanical properties. In fact, sulfone-based poly(arylene ether)s have gained considerable commercial and industrial importance. Aromatic polymers that contain aryl ether or aryl sulfone linkages generally have lower glass-transition temperatures and greater chain flexibility than their corresponding polymers without these groups in the chain.[31–33] Also, it was well documented that aromatic sulfoxides are photochemically active molecules and characterisation of the triplet states of such simple organic molecules as PhEPh (E = S, SO, SO_2) has played a critical role in the development of their photochemistry and photophysics.[34,35]

In the present work we report the first examples of Group 10–12 metal–acetylide polymers and their dinuclear congeners containing O, S, SO and SO_2 functionalities. These represent unprecedented model systems to evaluate how the chalcogen-based conjugation interrupters would limit the effective conjugation length of polymetallaynes. The significance of the Group 16 residue in this class of materials in comparison to other conjugated linkers will be discussed.

Results and Discussion

Synthesis: The syntheses of bifunctional alkynylated precursors bearing 4,4′-diphenyl ether, 4,4′-diphenyl sulfide, 4,4′-diphenyl sulfoxide and 4,4′-diphenyl sulfone (abbreviated as H-T(O)T, H-T(S)T, H-T(SO)T, and H-T(SO_2)T, respectively) are outlined in Scheme 1. For H-T(O)T, 4,4′-bis[(trimethylsilyl)ethynyl]diphenyl ether was prepared by Pd/Cu-cat-

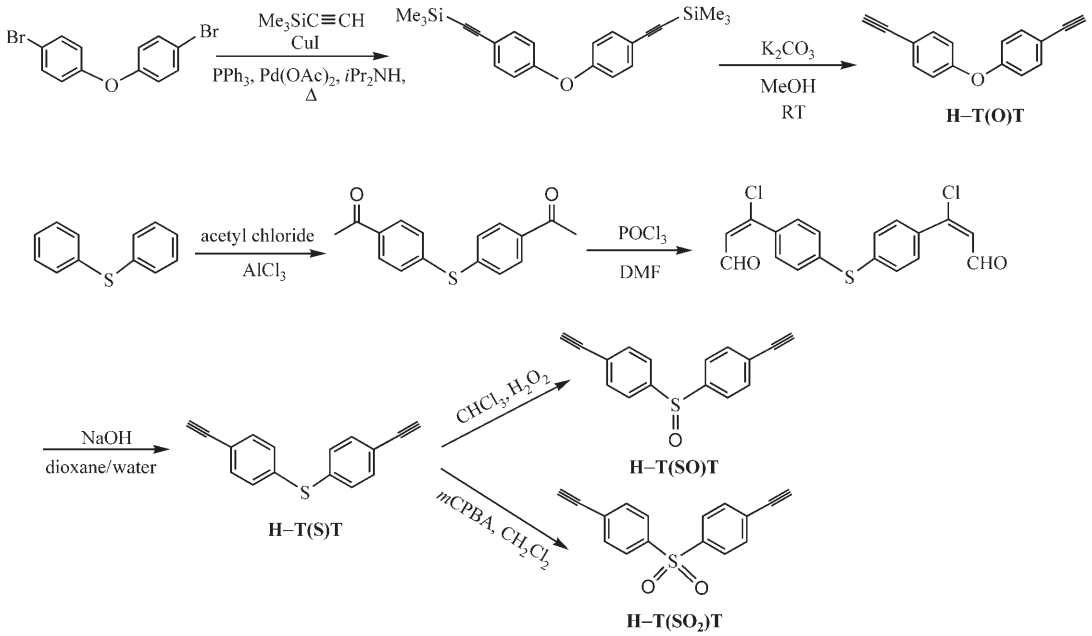

Scheme 1. Synthesis of the chalcogen-based diethynyl ligand precursors.

alyzed coupling of $Me_3SiC{\equiv}CH$ to 4,4′-dibromodiphenyl ether followed by removal of the TMS protecting group using a catalytic quantity of KOH in MeOH to yield 4,4′-diethynyldiphenyl ether. For H-T(S)T, diphenyl sulfide was treated with acetyl chloride and aluminium chloride to afford the corresponding diketone. Phosphoryl chloride was then mixed with the diketone in DMF to give the dialdehyde that further reacted with NaOH in a dioxane/water mixture to give 4,4′-diethynyldiphenyl sulfide. 4,4′-Diethynyldiphenyl sulfide was used as the starting material for making H-T(SO)T and H-T(SO_2)T through two different oxidation pathways. The ligand precursors with the sulfoxide and sulfone groups were obtained by employing 30% hydrogen peroxide and *m*-chloroperoxybenzoic acid (*m*CPBA), respectively, as the oxidizing agents. All attempts to produce H-T(SO_2)T from H-T(S)T by using an excess of or highly concentrated H_2O_2 failed. The crude products from these reaction mixtures were purified by passage through short columns of silica gel and were recrystallised where necessary.

Scheme 2 shows the chemical structure and the synthetic strategies for the metal complexes in the present study. The as-prepared diethynyl synthons were used to form a series of Group 10–12 metallaynes and metallopolymers by adaptation of the reported dehydrohalogenation procedures.[23,24] The triple bonds are represented by T and the diphenyl ether, sulfide, sulfoxide, and sulfone by O, S, SO and SO_2, respectively. Model metal diynes and polyynes are differentiated by use of the subscript ∞ for the polyynes. The feed mole ratios of the platinum chloride precursors and the diethynyl ligands were 2:1 and 1:1 for the diyne and polyyne syntheses, respectively. The diplatinum compounds were isolated by preparative TLC on silica. Purification of the polymers was accomplished by silica column chromatography with CH_2Cl_2 as the eluent, and they were all obtained in high purity. Likewise, the diethynyl precursors were used to form dinuclear alkynyl complexes of Au^I and Hg^{II} through the reaction between the appropriate bis-alkynes and Au(PPh_3)Cl or MeHgCl in the presence of a base.[36] The yields of these transformations were high in each case. All the new complexes and polymers are air-stable and can be stored without any special precautions. They are found to be soluble in chlorinated solvents such as CH_2Cl_2 but are generally insoluble in hydrocarbons. They all gave satisfactory analytical data, and were characterised by fast-atom-bombardment mass spectrometry (FAB-MS), and IR and NMR spectroscopy.

Chemical characterisation: The spectroscopic data given in the Experimental Section are in line with their assigned structures. All the compounds possess a well-defined size and structure. The IR spectra are each characterised by a sharp ν(C≡C) absorption band at aproximately 2090–2138 cm^{-1}. The compounds with the sulfoxide and sulfone groups show sharp ν(SO) and ν-(SO_2) absorption bands at about 1040–1049 and 1151–1156 cm^{-1}, respectively. The formulae of the binuclear complexes were all successfully established by using the intense molecular-ion peaks in their respective positive FAB mass spectra. The NMR spectra were indicative of the highly symmetrical structure of the binuclear complexes and also revealed a high degree of structural regularity in the polymers. The single $^{31}P\{^1H\}$ NMR signals flanked by platinum satellites for the platinum complexes and polymers were consistent with a *trans* geometry of the square-planar Pt unit with the ^1J(P,Pt) values typical of those for related *trans*-PtP_2 systems.[23,24] In all cases, ^1H NMR resonances arising from the protons of the organic moieties were observed. Notably, two distinct ^{13}C NMR signals for the α- and β-acetylenic carbon atoms were ob-

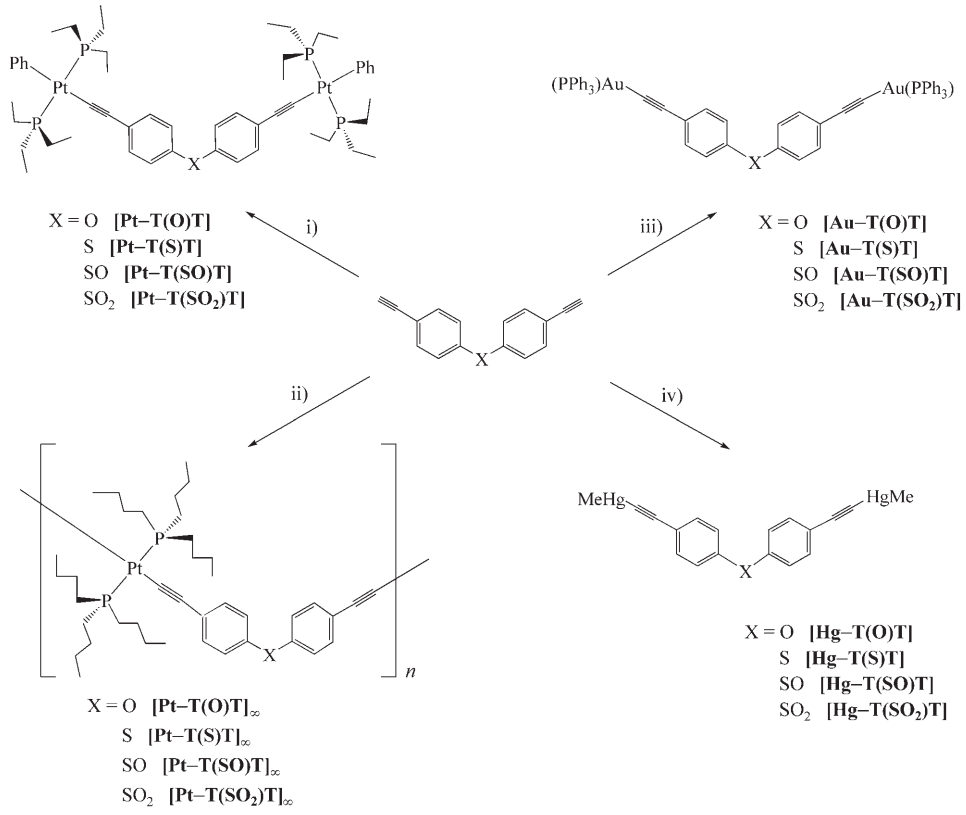

Scheme 2. Synthesis of the platinum(II), gold(I) and mercury(II) alkynyls. i) *trans*-[PtPh(Cl)(PEt_3)$_2$] (2 equiv), CuI, *i*Pr_2NH, RT; ii) *trans*-[$PtCl_2$(PBu_3)$_2$] (1 equiv), CuI, *i*Pr_2NH, RT; iii) [Au(PPh_3)Cl] (2 equiv), NaOH/MeOH, RT; iv) [MeHgCl] (2 equiv), NaOH/MeOH, RT.

served, and the α-acetylide chemical shifts were shifted downfield with respect to the free dialkyne, in agreement with the formation of a metal–C(sp) σ bond.

The three-dimensional molecular structures of selected dinuclear complexes were confirmed by X-ray crystallography (Figures 1–3). Pertinent bond lengths and angles are given in Tables 1–3. All of these molecules were shown to adopt angular geometry at the sp^3-hybridised heteroatom. For the platinum complexes, the coordination geometry at each Pt centre is square-planar with the two PEt_3 groups *trans* to each other and the metal capping groups are connected by the three diethynyl ligands. The C≡C bond lengths are characteristic of metal–alkynyl σ bonding and the bond angles of the Pt–C≡C units in the range of 173.0(8)–178.1(7)° conform to the rigid-rod nature of these molecules. In [Au-T(O)T], the Au–P bond lengths are typical at 2.2754(12) and 2.2702(15) Å,[36c] but appear longer than those of the chloro-gold(I) phosphine complexes; a fact ascribed to the stronger

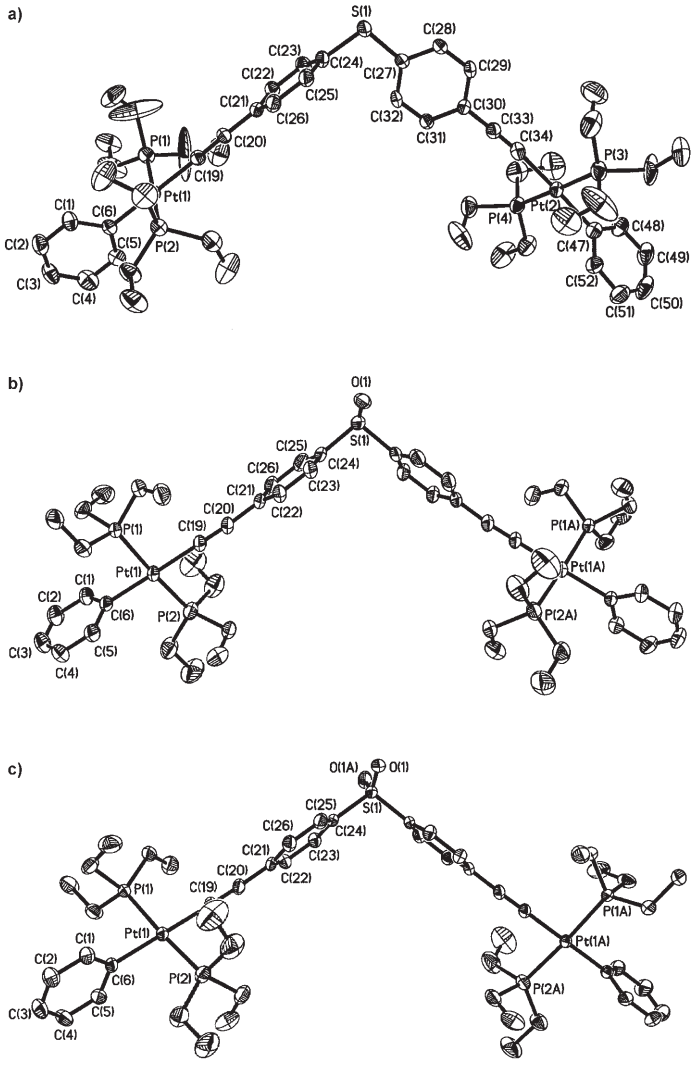

Figure 1. X-ray crystal structures of: a) [Pt-T(S)T], b) [Pt-T(SO)T] and c) [Pt-T(SO_2)T]. Thermal ellipsoids were drawn at the 25% probability level. All hydrogen atoms were omitted for clarity.

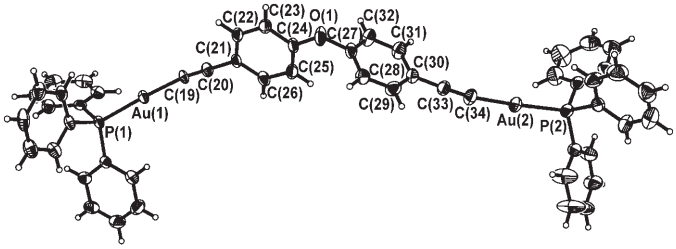

Figure 2. X-ray crystal structure of [Au-T(O)T]. Thermal ellipsoids were drawn at the 25% probability level.

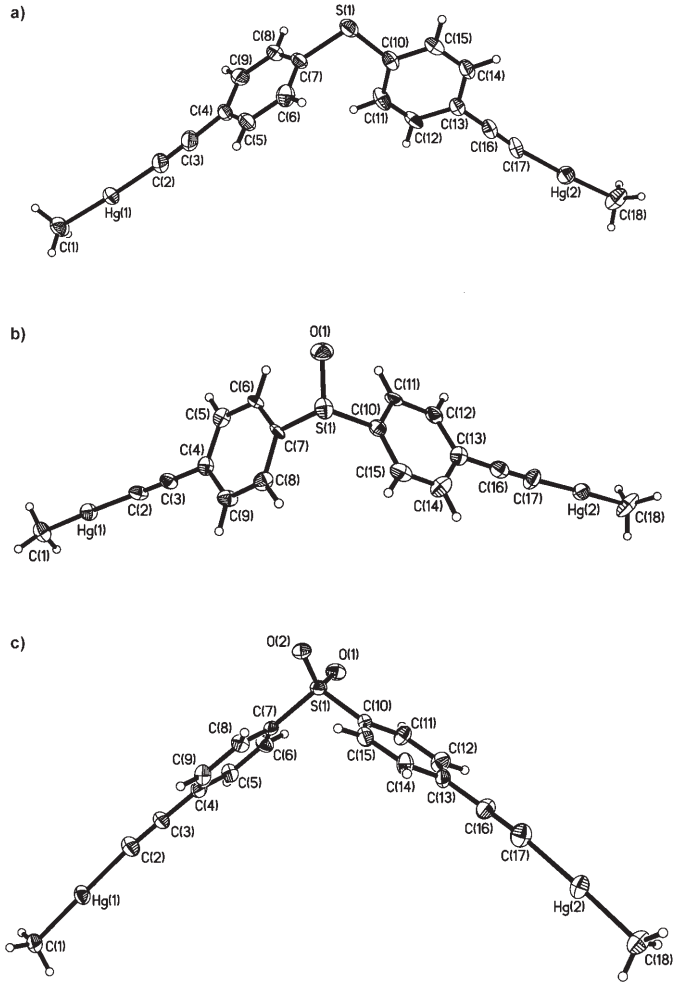

Figure 3. X-ray crystal structures of: a) [Hg-T(S)T], b) [Hg-T(SO)T] and c) [Hg-T(SO_2)T]. Thermal ellipsoids were drawn at the 25% probability level.

trans influence of the alkynyl group as compared to that of the chloro group. The Au–C bond lengths span the narrow range of 1.991(6)–2.025(4) Å. The geometry about the Au^I centre is essentially linear, and the P-Au-C angles are 174.23(13) and 177.12(17)°. As the bulky PPh_3 ligands prevent the close approach of adjacent molecules, no Au···Au intermolecular contacts are apparent in this case. For the organomercurials, the Hg–C≡C units are nearly linear with

Table 1. Selected bond lengths [Å] and angles [°] for [Pt-T(S)T], [Pt-T(SO)T] and [Pt-T(SO_2)T].

	[Pt-T(S)T]	[Pt-T(SO)T]	[Pt-T(SO_2)T]
Pt(1)−P(1)	2.287(2)	2.2971(16)	2.2977(12)
Pt(1)−P(2)	2.289(2)	2.2869(17)	2.2888(13)
Pt(1)−C(6)	2.053(7)	2.073(5)	2.075(4)
Pt(1)−C(19)	2.017(8)	2.011(5)	2.009(4)
Pt(2)−P(3)	2.275(2)		
Pt(2)−P(4)	2.286(2)		
Pt(2)−C(34)	2.020(9)		
Pt(2)−C(47)	2.057(8)		
C(19)−C(20)	1.201(9)	1.195(7)	1.201(6)
C(33)−C(34)	1.225(10)		
S(1)−C(24)	1.763(8)	1.793(6)	1.766(4)
S(1)−C(27)	1.769(8)		
S(1)−O(1)		1.378(12)	1.432(4)
P(1)-Pt(1)-P(2)	174.16(8)	175.73(6)	174.81(5)
P(1)-Pt(1)-C(19)	89.2(2)	91.63(16)	91.49(13)
P(2)-Pt(1)-C(19)	88.8(2)	86.46(17)	86.49(13)
P(3)-Pt(2)-P(4)	177.85(10)		
P(3)-Pt(2)-C(34)	90.0(2)		
P(4)-Pt(2)-C(34)	89.6(2)		
Pt(1)-C(19)-C(20)	178.1(7)	175.8(6)	176.5(5)
Pt(2)-C(34)-C(33)	173.0(8)		
C(19)-C(20)-C(21)	175.5(9)	175.6(7)	176.5(6)
C(30)-C(33)-C(34)	178.5(9)		
$C(sp^2)$-S(1)-$C(sp^2)$	102.7(4)	100.0(4)	106.2(3)
C(24)-S(1)-O(1)		111.9(5)	106.7(2)
O(1)-S(1)-O(1A)			121.1(4)

Table 2. Selected bond lengths [Å] and angles [°] for [Au-T(O)T].

Au(1)−P(1)	2.2754(12)	Au(1)−C(19)	2.025(4)
Au(2)−P(2)	2.2702(15)	Au(2)−C(34)	1.991(6)
C(19)−C(20)	1.167(6)	C(33)−C(34)	1.203(8)
C(24)−O(1)	1.364(6)	C(27)−O(1)	1.413(6)
P(1)-Au(1)-C(19)	174.23(13)	Au(1)-C(19)-C(20)	167.4(4)
P(2)-Au(2)-C(34)	177.12(17)	Au(2)-C(34)-C(33)	171.7(5)
C(24)-O(1)-C(27)	119.5(4)		

Table 3. Selected bond lengths [Å] and angles [°] for [Hg-T(S)T], [Hg-T(SO)T], and [Hg-T(SO_2)T].

	[Hg-T(S)T]	[Hg-T(SO)T]	[Hg-T(SO_2)T]
Hg(1)−C(1)	2.065(12)	2.023(15)	2.065(11)
Hg(1)−C(2)	2.011(14)	2.031(13)	2.043(12)
Hg(2)−C(17)	2.045(14)	2.036(13)	2.052(12)
Hg(2)−C(18)	2.044(15)	2.106(16)	2.043(10)
C(2)−C(3)	1.211(18)	1.193(18)	1.199(15)
C(16)−C(17)	1.191(17)	1.200(19)	1.193(14)
S(1)−C(7)	1.776(10)	1.752(12)	1.768(9)
S(1)−C(10)	1.766(13)	1.819(12)	1.759(9)
S(1)−O(1)		1.503(11)	1.447(7)
S(1)−O(2)			1.447(7)
C(1)-Hg(1)-C(2)	176.9(6)	177.8(6)	179.5(5)
C(17)-Hg(2)-C(18)	177.2(6)	177.3(7)	176.8(5)
Hg(1)-C(2)-C(3)	176.6(13)	178.9(12)	175.5(11)
Hg(2)-C(17)-C(16)	172.0(11)	174.7(12)	175.6(12)
C(7)-S(1)-C(10)	102.6(5)	99.7(6)	106.8(5)
C(7)-S(1)-O(1)		105.3(6)	107.5(5)
C(7)-S(1)-O(2)			107.9(4)
O(1)-S(1)-O(2)			119.3(4)

the Hg-C-C angles being 172.0(11)–178.9(12)°. Examination of the crystal packing diagram for each dimercury complex shows the involvement of ligand-unsupported mercuriophilicity in its structure. The lattice is stabilized by various weak intermolecular noncovalent Hg···Hg interactions (4.130–4.147 for [Hg-T(S)T], 3.671–4.202 for [Hg-T(SO)T], and 3.621–4.343 Å for [Hg-T(SO_2)T]). Although each of these mercuriophilic contacts is relatively weak, it is the large number of them that play a supramolecular role and generate a significant driving force for the solid-state aggregation. We believe that such mercuriophilic forces are more than just van der Waals interactions in these solid-state systems. The van der Waals radius of mercury has been debated and a value of up to 2.2 Å has been proposed recently,[37] and is predicted to be a better estimate than the value quoted by Bondi.[38] Here, the observed Hg···Hg separations are comparable to the values of 3.71–4.25 Å for [Hg(C≡CR)$_2$] (R = Ph, $SiMe_3$),[39] and 4.077 and 4.449 Å computed for molecular $(HgH_2)_n$ clusters (n = 2, 3),[40] and are towards the upper limit of those accepted as representing metallophilic interactions.[41] None of these structures show π–π stacking of the arene rings in the solid state.

Structural and thermal properties of polymers: The thermal properties of the polymers were examined by thermogravimetric analysis (TGA) and differential scanning calorimetry (DSC) under nitrogen (Table 4). Analysis of the TGA trace for the four Pt^{II} polymers shows that they all exhibit good thermal stability. It has long been recognised that aromatic polymers containing aryl ether or sulfone linkages have excellent thermal and mechanical properties.[28] These platinum polyynes, with different heteroatoms as the linkage groups, retain greater than 95% of their mass under N_2 up to 335–363 °C. The temperatures at which decomposition begins appear higher than those in related polymers *trans*-[{−Pt(PBu_3)$_2$C≡C(p-C_6H_4)$_m$C≡C−}$_n$] (m = 1, 2, at ~300 °C).[8b] Thus, the introduction of heteroatoms can definitely increase the thermal stability of this class of metal polyynes. We observe a sharp weight loss of 28% for [Pt-T(O)T]$_\infty$ whereas 40% of the weight was lost for [Pt-T(S)T]$_\infty$, [Pt-T(SO)T]$_\infty$ and [Pt-T(SO_2)T]$_\infty$. The decomposition step is ascribed to the removal of one PBu_3 group from [Pt-T(O)T]$_\infty$ and the loss of six Bu groups from each of the latter three polymers. These platinum polymers also reveal no discernible glass transitions in the DSC curves.

Table 4. Structural and thermal properties of platinum polyynes.

Polymer	M_n	M_w	M_w/M_n	T_{decomp}(onset) [°C]
[Pt-T(O)T]$_\infty$	12750	37390	2.93	363 ± 5
[Pt-T(S)T]$_\infty$	7020	11430	1.63	361 ± 5
[Pt-T(SO)T]$_\infty$	6550	11100	1.69	354 ± 5
[Pt-T(SO_2)T]$_\infty$	7930	15480	1.95	335 ± 5

The molecular weight data of our polymers, as determined in THF by gel-permeation chromatography (GPC), are shown in Table 4. The degree of polymerization calculated

from M_w are 46, 14, 13 and 18 for [Pt-T(O)T]$_\infty$, [Pt-T(S)T]$_\infty$, [Pt-T(SO)T]$_\infty$ and [Pt-T(SO$_2$)T]$_\infty$, respectively. It should be noted that GPC does not give absolute values of molecular weights, but provides a measure of hydrodynamic volume. Rodlike polymers in solution possess different hydrodynamic properties than flexible polymers. So, calibration of the GPC with polystyrene standards is likely to inflate the values of the molecular weights of the polyynes to some extent. However, the lack of discernible resonances that could be attributed to end groups in the NMR spectra offers good support for the macromolecular nature of these polyynes.

Photophysical properties: The absorption and emission data of the new metalated compounds are shown in Table 5. All the metal alkynyls display similarly structured absorption bands in the near UV region and the dependence of the absorption energies on the ligand type would suggest that the absorption pattern is dominated by intraligand ^{1}IL (π–π^*) transitions associated with the arylene–ethynylene moiety from the S_0 to S_1 levels, possibly mixed with some admixture of metal orbitals. Coordination of metal to the organic system results in enhanced $\pi\rightarrow\pi^*$ transitions. As compared with the metal-free alkynes, we note that the position of the lowest energy absorption band experiences a red-shift after the inclusion of a metal fragment in all of these metal alkynyls. This reveals that π conjugation is preserved through the metal site by mixing of the frontier orbitals of the metal and ligand. A simple glance tells us that the extent of π conjugation of our metalated compounds follows the order Pt > Au > Hg according to the absorption data. Also, the transition energies of the platinum polymers are lowered with respect to those of the diplatinum complexes, suggesting a well-extended singlet excited state in the Pt^{II} polyynes. Generally speaking, the absorption energy of the oxygen-linked metal compound is the largest for each metal type, whereas the sulfone-containing counterpart shows the lowest absorption energy. In energy terms, the experimentally determined HOMO–LUMO energy gaps (E_g) as measured from the onset wavelength in the solid-film state are also shown in Table 5. With reference to the similarly prepared bi(*p*-phenylene)-linked compounds [MeHgC≡C(*p*-C$_6$H$_4$)$_2$C≡CHgMe] (309 nm), [(Ph$_3$P)AuC≡C(*p*-C$_6$H$_4$)$_2$C≡CAu(PPh$_3$)] (326 nm), *trans*-[Pt(Ph)(PEt$_3$)$_2$C≡C(*p*-C$_6$H$_4$)$_2$C≡CPt(Ph)(PEt$_3$)$_2$] (349 nm), and *trans*-[{−Pt(PBu$_3$)$_2$C≡C(*p*-C$_6$H$_4$)$_2$C≡C−}$_n$] (372 nm), we find that the non-π-conjugated chalcogen unit between the two phenyl rings hinders conjugation and causes a blue-shift in the absorption wavelength (280–300, 303–318, 325—345 and 343–361 nm for our Hg, Au and Pt dinuclear complexes, and Pt polymers, respectively). In other words, the energy of the S_1 singlet state (or the E_g value) can be modified simply by varying the electronic properties of the spacer group; this is vital for governing the efficiency of triplet-state emission (vide infra).

The thin-film photoluminescence (PL) spectra of the metal alkynyls were probed at various temperatures (Table 5, and Figures 4 and 5). Upon photoexcitation, we observed an intense purple-blue ^{1}(π–π^*) fluorescence emission peak ($S_1\rightarrow S_0$) near 400 nm in dilute fluid solutions at 290 K for each of them in agreement with the small Stokes shift observed. We have shown that the organic triplet emissions of our compounds with large optical gaps have been illuminated by the heavy-atom effect of Group 10–12 transition-metal elements. As the temperature was gradually decreased, we observed virtually no fluorescence band, but only the prominent phosphorescence band emanating

Table 5. Photophysical data for the metal diynes and polyynes.

	λ_{max} [nm][a]		E_g [eV][b]	λ_{em} [nm][c]	
	CH_2Cl_2	Film		CH_2Cl_2[d] (290 K)	Film (20 K)
[H-T(O)T]	260 (1.6)	270	4.13	333, 344 (3.96, 1.64)	-
[H-T(S)T]	244 (2.5), 278 (2.7), 303* (1.5)	288	3.65	332, 346 (2.46, 1.94)	-
[H-T(SO)T]	241* (2.5), 268 (3.9)	244*, 270	4.12	334, 341 (2.32, 1.61)	-
[H-T(SO$_2$)T]	249* (2.2), 270 (3.3)	259, 278, 290*	3.62	304 (9.10, 1.32)	-
[Pt-T(O)T]	269 (6.2), 292 (7.0), 325 (8.1)	267, 291, 326	3.63	368*, 375*, 421 (0.10, 1.57)	448, 468, 493
[Pt-T(S)T]	297 (4.5), 334 (6.1)	272*, 296, 334	3.39	386 (0.25, 1.06)	373*, 483, 509*, 521*, 536*
[Pt-T(SO)T]	249* (3.5), 304 (6.8), 333 (9.5)	271*, 304, 333	3.43	372*, 392 (0.33, 1.17), 407*	469, 495*
[Pt-T(SO$_2$)T]	305* (5.6), 345 (10.3)	347	3.24	370 (0.79, 1.43)	465, 489*, 499*, 513*
[Pt-T(O)T]$_\infty$	267, 292, 343	266, 291, 337	3.40	368 (0.10, 1.72), 492*	454, 475, 488
[Pt-T(S)T]$_\infty$	269*, 296, 352	294, 344	3.26	382 (0.25, 0.78), 482*	484, 510*, 522*, 537*
[Pt-T(SO)T]$_\infty$	272*, 299, 349	266*, 299, 337	3.28	382 (0.16, 0.98), 474*	475, 501*, 527*
[Pt-T(SO$_2$)T]$_\infty$	270*, 301*, 361	268*, 301*, 350	3.18	389 (0.20, 1.35), 481	484, 509*, 536*
[Au-T(O)T]	275* (8.1), 289 (10.9), 303 (11.4)	277*, 293, 311	3.67	391 (0.59, 1.39), 430*	445, 474
[Au-T(S)T]	277* (4.9), 300 (6.0), 313 (6.3)	278*, 319	3.41	384 (0.88, 1.30)	477, 509, 530*
[Au-T(SO)T]	294 (12.0), 307 (12.8)	298, 313	3.62	365, 382 (1.17, 1.26)	473, 493*, 523*
[Au-T(SO$_2$)T]	269* (4.8), 286* (6.8), 308 (8.7), 318 (9.4)	271*, 295*, 311, 324	3.39	388 (0.37, 0.93)	466, 500*, 515*
[Hg-T(O)T]	280 (6.9)	294	3.82	392 (1.77, 1.14), 416*	372*, 396*, 440, 470, 504*
[Hg-T(S)T]	264* (3.8), 290 (4.8)	275*, 310	3.48	395 (2.60, 1.12), 418*	399*, 428*, 478, 495, 503*
[Hg-T(SO)T]	279* (8.6), 289 (9.8)	285*, 302	3.69	363*, 384 (9.32, 1.22), 424*	375*, 394*, 452, 480, 495*, 544*
[Hg-T(SO$_2$)T]	266* (5.1), 291 (5.9), 300 (5.9)	290*, 310	3.46	385 (2.72, 1.14)	375*, 385*, 448, 469*, 481*

[a] Extinction coefficients (10^4 M^{-1} cm^{-1}) are shown in parentheses. [b] Estimated from the onset wavelength of the solid-state optical absorption. [c] Asterisks indicate emission peaks appear as shoulders or weak bands. [d] Fluorescence quantum yields [%] and lifetimes [ns] shown in parentheses (ϕ_F, τ_F) are measured in CH_2Cl_2 relative to anthracene.

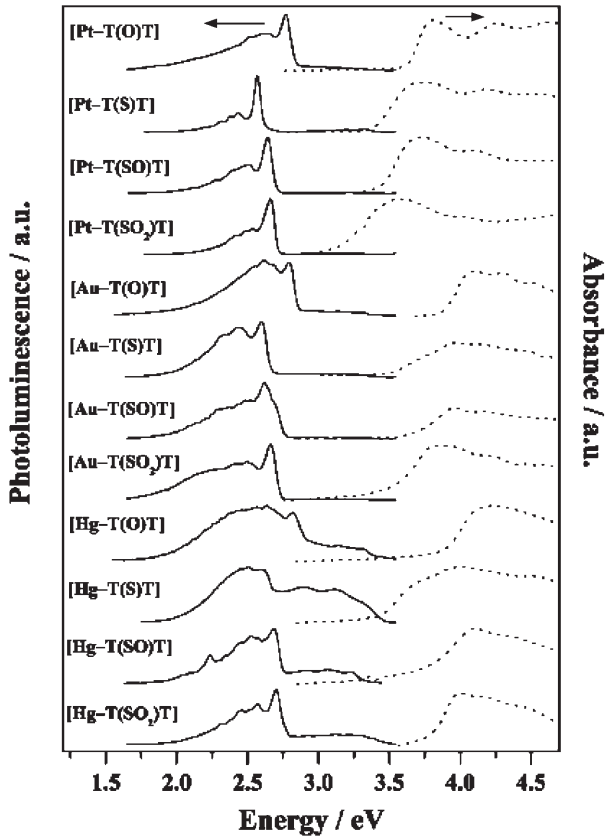

Figure 4. The photoluminescence (——) and absorption (-----) spectra of thin films of binuclear complexes of Pt, Au and Hg taken at 20 and 290 K, respectively.

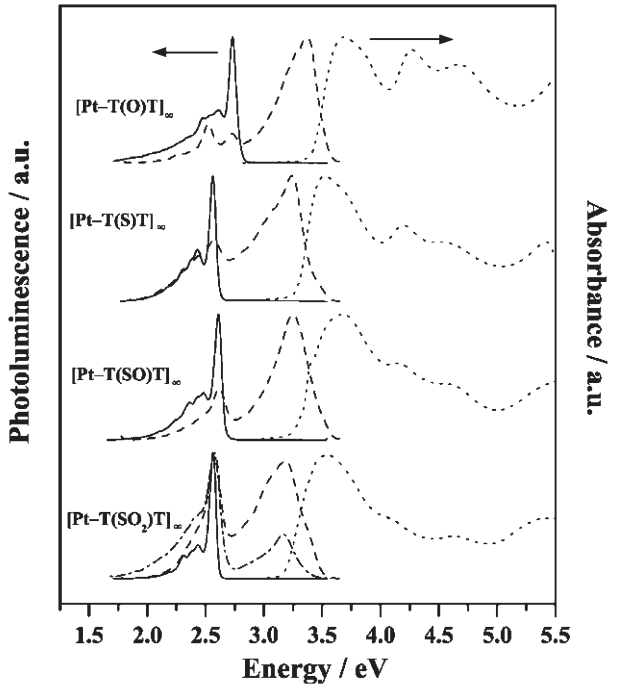

Figure 5. The photoluminescence (PL) and absorption spectra of Pt polyynes. The absorption spectra are the dotted lines at higher energy measured at 290 K. PL spectra were taken at both 290 (-----, in CH_2Cl_2) and 20 K (——, as thin films). For the polyyne [Pt-T(SO_2)T]$_\infty$, the 290 K PL spectrum (–•–•) measured as a thin film is also given.

mainly from the central ligand chromophore. At 20 K, the principal emissive peaks in the low-lying region that exhibited large Stokes shifts from the absorption spectra (Figures 4–6) possessed long emission lifetimes indicative of their triplet parentage. The emission maxima are dependent on the nature of the acetylide ligand and thus the lowest emissive states in these compounds can tentatively be assigned as metal-perturbed ^{3}IL (π–π^*) transitions. The emission assignment can also be interpreted in terms of the observed temperature dependence of the PL data. Representative examples of the temperature dependencies of the PL spectra for the model compounds and polymers are displayed in Figure 6. In each case, when the temperature is lowered, the triplet emission band increases in intensity; this change is accompanied by a well-resolved vibronic structure with most weight in the 0–0 vibrational peak, diagnostic of the involvement of ^{3}IL (π–π^*) excited states. Such an increase in intensity indicates a long-lived triplet excited state that is more sensitive to thermally activated nonradiative decay mechanisms.[7b] The phosphorescence lifetimes at the peak maxima are found to be in the microsecond regime (0.12–13.6 μs) at 20 K, typical of those observed in similar polymetallaynes reported.[23,24] While we have a long-term interest to observe triplet emission under ambient conditions, this work is attractive in that room-temperature phosphorescence can be clearly identified for our platinum polymers (see Figure 5) and is rarely found in the literature for related systems containing heteroaromatic spacers. Presumably due to the internal heavy-atom effect of the sulfone group, [Pt-T(SO_2)T]$_\infty$ shows the most intense phosphorescence band at 290 K among the four polymers and we can even observe very strong solid-state triplet emission for [Pt-T(SO_2)T]$_\infty$ in which the ratio of integrated intensities of phosphorescence to fluorescence is greater than unity.

To examine the spatial extent of the singlet and triplet excitons in our systems, we have constructed the energy level scheme for the lower lying excitations (Figure 7) based on the absorption and PL data. The energy values are absolute values with respect to the S_0 ground state. For the Pt^{II} systems, the lowest T_1 state essentially remains strongly localised, as can be inferred from the small energy difference between triplet emissions in the metal diynes and polyynes. Previous calculations performed for *trans*-[{–Pt(PBu_3)$_2$C≡C-(*p*-C_6H_4)C≡C–}$_n$] (abbreviated as [Pt-T(P)T]$_\infty$) also indicated the triplet to be confined to the phenylene ring.[42] Substitution of the metal groups does not seem to alter this strong confinement. All these efficient phosphorescent metal–organic systems containing the conjugation-interrupting Group 16 elements exhibit T_1–S_0 gaps of 2.5 eV or above, corresponding to S_1(PL)–S_0 gaps of around 3.13–3.57 eV. The measured $\Delta E(S_1–T_1)$ values for our present systems are constant at around 0.7 ± 0.1 eV, corresponding closely to the S_1–T_1 energy gaps estimated for some organic conjugated

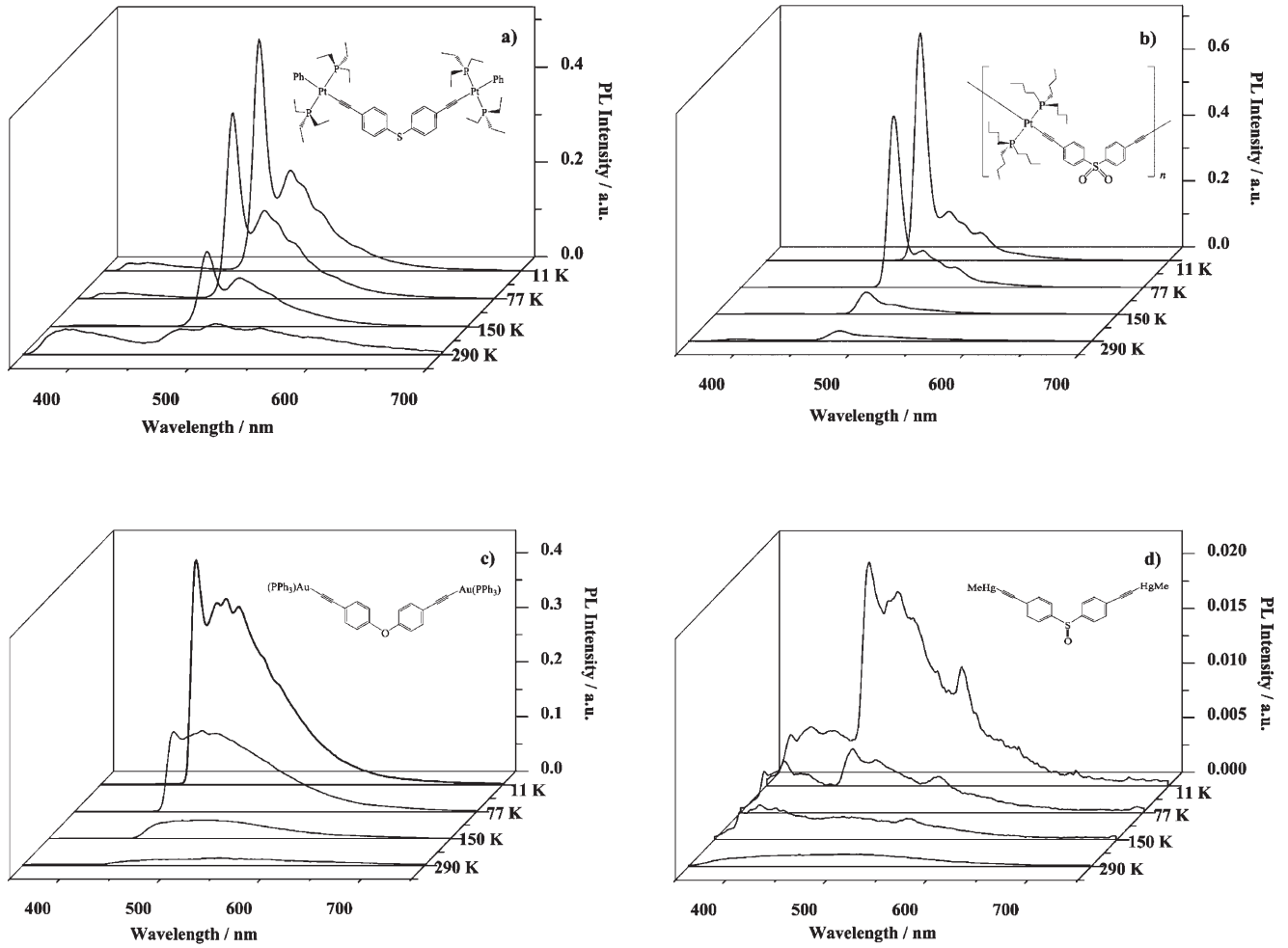

Figure 6. Temperature dependence of the PL of: a) [Pt-T(S)T], b) [Pt-T(SO_2)T]$_\infty$, c) [Au-T(O)T] and d) [Hg-T(SO)T].

polymers.[43,44] We ascribe such a constant $\Delta E(S_1–T_1)$ value to the exchange energy and possibly some additional constant contribution due to the admixture of the metal orbitals. All of the sulfides have triplet energies lower than the corresponding sulfoxides, whereas those of the sulfones are typically higher than those of the sulfoxides. These observations agree with some small-molecule, organic, aromatic molecules ArEAr (Ar = aryl, E = S, SO, SO_2). From experiment, the T_1–S_0 gap generally changes with the E unit in the order O > SO_2 > SO > S for the metal diynes. However, the T_1 level for [Pt-T(SO_2)T]$_\infty$ appears to be slightly lower than those of [Pt-T(S)T]$_\infty$ and [Pt-T(SO)T]$_\infty$, probably because of its higher degree of polymerization (DP ~ 18) than the last two (~13–14). With the same ligand chromophore, the T_1 levels for the Pt^{II} and Au^{I} compounds are in general higher than those of the corresponding Hg^{II} congener. Hindered conjugation by using different Group 16 element derived units shifts the phosphorescence to the blue relative to the conjugated biphenyl-spaced counterparts and the extent of blue shift is the largest for the diphenyl ether derivatives (approximately 0.44–0.48 eV).

With the assumption that the ISC efficiency is close to unity for third-row transition-metal chromophores,[45,46] the radiative $(k_r)_P$ and nonradiative $(k_{nr})_P$ decay rate constants are calculated from the measured lifetime of triplet emission (τ_P) and the phosphorescence quantum yield (ϕ_P) by the relationships: $(k_{nr})_P = (1-\phi_P)/\tau_P$ and $(k_r)_P = \phi_P/\tau_P$. Table 6 shows the relevant data for these photophysical parameters. Generally, we observe a rather strong dependence of ϕ_P with the heavy-metal perturbation effect and the value of ϕ_P follows the order $Pt^{II} > Au^{I} > Hg^{II}$, and the Pt polyynes give more efficient phosphorescence than the Pt diynes; however, ϕ_P does not vary much with the type of E group in the present study. For phosphorescence in aromatic hydrocarbon molecules, k_r is typically found to be between 0.1 and 1 s^{-1}.[47] So, the heavy-atom effect of Pt, Au and Hg increases the radiative decay rate for the triplet emission by four orders of magnitude. Comparing the $(k_r)_P$ and $(k_{nr})_P$ values for the individual metal polyynes and diynes with T_1–S_0 gaps of 2.5 eV or above it can be seen that the values for $(k_{nr})_P$ are comparable to those for $(k_r)_P$. For instance, insertion of the Group 16 conjugation interrupters in the Pt polyyne systems results in $(k_r)_P$ values of $(5.4–8.1)\times10^4$ s^{-1} that are more efficient relative to [Pt-T(P)T]$_\infty$ ($(k_r)_P = 6\times10^3$ s^{-1} at 20 K) by about one order of magnitude.[23a] Our findings corroborate the assertion that high-energy triplet states (and concurrent-

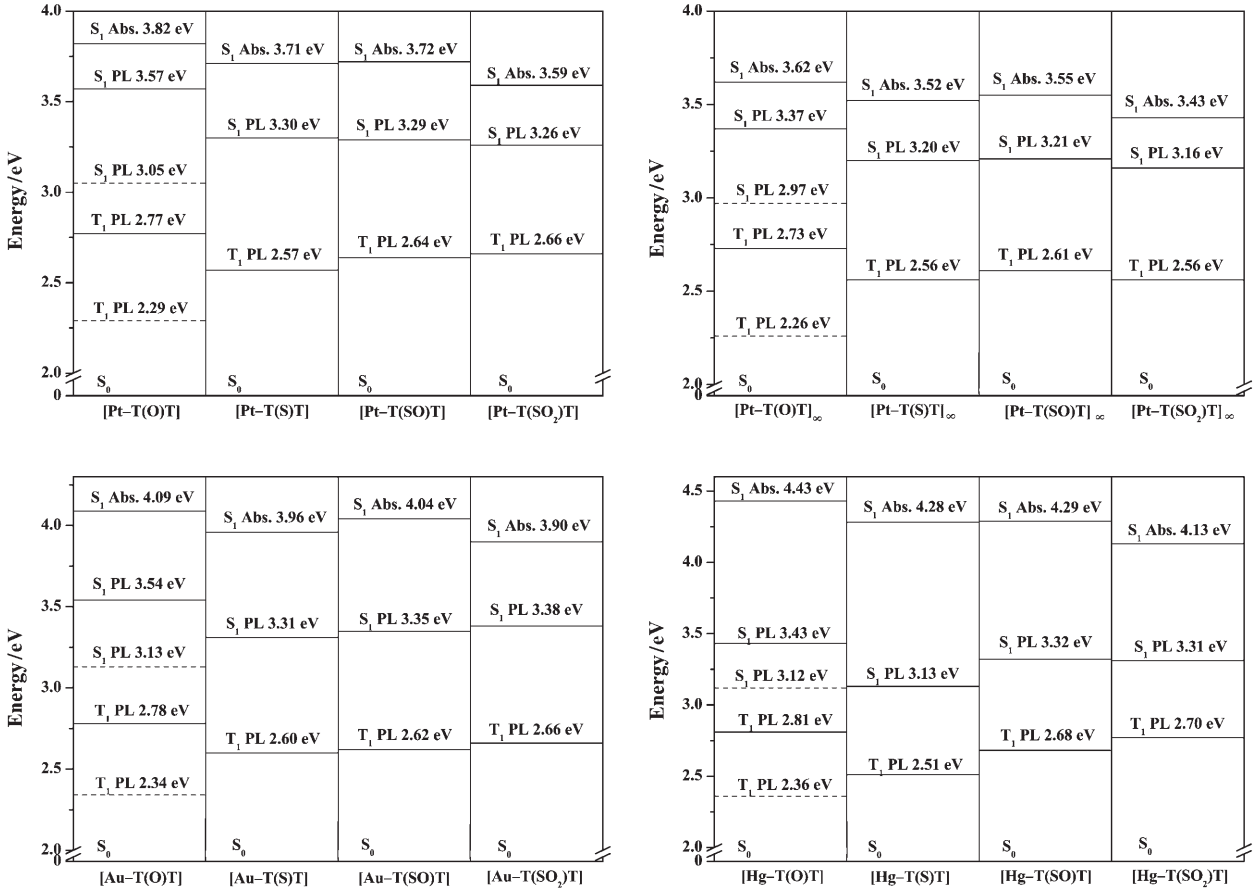

Figure 7. Electronic energy level diagram of metal diynes and polyynes containing Group 16 main-group elements determined from absorption and PL data. Dashed lines represent the levels for the metal diynes and polyyne containing the bi(*p*-phenylene) spacer. The S_0 levels are arbitrarily shown to be of equal energy.

Table 6. Some photophysical parameters for the phosphorescence emission at 20 K.

	$E(T_1–S_0)$ [eV]	ϕ_p [%]	τ_P [μs]	$(k_r)_P$ ($\times 10^4$) [s^{-1}]	$(k_{nr})_P$ ($\times 10^4$) [s^{-1}]	τ_r [μs][a]
[Pt-T(O)T]	2.77	25.9	6.21	4.18	11.9	24.0
[Pt-T(S)T]	2.57	24.8	11.6	2.13	6.48	46.8
[Pt-T(SO)T]	2.64	27.6	7.49	3.68	9.67	27.1
[Pt-T(SO_2)T]	2.66	20.8	13.6	1.52	5.81	65.4
$[Pt-T(O)T]_\infty$	2.73	45.8	6.38	7.18	8.50	13.9
$[Pt-T(S)T]_\infty$	2.56	48.6	6.02	8.08	8.54	12.4
$[Pt-T(SO)T]_\infty$	2.61	51.3	7.27	7.06	6.69	14.2
$[Pt-T(SO_2)T]_\infty$	2.56	46.3	8.57	5.41	6.26	18.5
[Au-T(O)T]	2.78	19.6	3.38	5.79	23.8	17.2
[Au-T(S)T]	2.60	16.2	12.2	1.33	6.88	75.3
[Au-T(SO)T]	2.62	18.4	3.75	4.91	21.8	20.4
[Au-T(SO_2)T]	2.66	17.0	11.6	1.47	7.17	68.2
[Hg-T(O)T]	2.64	5.39	0.93	5.80	101.7	17.3
[Hg-T(S)T]	2.51	6.69	0.34	19.8	274.4	5.08
[Hg-T(SO)T]	2.56	6.54	0.12	54.5	778.8	1.83
[Hg-T(SO_2)T]	2.58	4.98	0.20	24.9	475.1	4.02

[a] The radiative lifetimes (τ_r) of the triplet excited state are deduced from $\tau_r = \tau_P/\phi_P$.

ly large optical gaps) intrinsically lead to the more efficient phosphorescence in metal-containing arylene–ethynylenes. Hence, the successful use of chalcogen-containing conjugation interrupters in such metal polyynes can limit the effective conjugation length and gives rise to efficient crossover between S_1 and T_1 states.

We now compare the nonradiative decay of Pt diynes and polyynes. Despite the fact that the same organic groups are available for nonradiative decay in the metal polyynes and diynes, it is possible to identify factors that may lead to different nonradiative behaviour. First of all, comparing the PL spectra of platinum dimeric complexes and their corresponding polymers, it can be seen that there is consistently more weight in the vibronic side peaks of the triplet emission of the dimer than in the phosphorescence band of the polymer. This suggests that there is less overlap between the vibrational levels of the ground and excited states, and therefore the triplet excited state in the dimer is more distorted than that in the polymer. Calculations carried out for $[Pt-T(P)T]_\infty$ and its dimeric analogue have also shown this to be the case. Secondly, since triplet excitons may diffuse along a polymer chain, there could be bimolecular nonradiative decay mechanisms such as triplet–triplet annihilation occurring for the polymer that cannot occur in the short-chain metal dimers. From Table 6, it is evident that, within the limits of experimental error, the Pt polymers and dimers

appear to have similar $(k_{nr})_P$ values. This is in agreement with the fact that the site of emission and thus the vibrations involved are the same. It also implies that any bimolecular quenching processes in the polymers play a lesser role than the vibrationally induced nonradiative decay.

Conclusion

A novel strategy is discussed that used a series of diethynyl-based chalcogen-bridged biarylenes for the synthesis of transition-metal-containing macromolecules and related model complexes. Their photoluminescent and electronic properties have been characterised in detail using optical methods. The spatial extent of spectroscopic singlet and triplet energies as a function of the nature of the heavy metals and central spacer groups is discussed in these metalated alkynyl systems. The following observations and conclusions can be made:

1) The phosphorescence of {−MC≡C(C_6H_4)E(C_6H_4)-C≡CM−}-type materials containing the conjugation-interrupting segment (M = Pt, Au, Hg; E = O, S, SO, SO_2) is very strong at low temperatures. All the three transition metals (Pt, Au and Hg) can exert heavy-atom effects in the enhancement of the ISC rate to harvest triplet state light energy. The observed triplet yields are the highest for Pt^{II} systems (0.21–0.28 for diynes and 0.46–0.51 for polyynes) among the three metal classes and the lowest for the Hg^{II} counterparts.
2) We consider that the Group 16 heteroatom is a good conjugation interrupter to limit the conjugation length. All the materials show high-energy triplet states of 2.5 eV or above, leading to very efficient triplet emission, in accord with the energy-gap law established for triplet states in similar metalated systems. The use of chalcogen atoms increases the accessibility of the $^3(\pi$–$\pi^*)$ excited states and allows the spin-forbidden phosphorescence to be easily observable even at room temperature for the Pt^{II} polymers.
3) Generally, the order of triplet energies for the dinuclear complexes is O > SO_2 > SO > S within each metal class, but the phosphorescence yield is relatively insensitive to the nature of the E group.
4) Reduced conjugation upon incorporation of these Group 16 elements markedly shifts the optical absorption and the phosphorescence band to the blue as compared to other metal polyynes with carbocyclic and heterocyclic spacers. For the Pt and Au systems, we are able to obtain comparable orders of magnitude for $(k_{nr})_P$ and $(k_r)_P$ which is rarely the case for polymetallaynes of this kind in the literature.
5) The results are significant with regard to fundamental understanding as well as providing design concepts for triplet-state light-emitting systems for use in optoelectronic research. This is desirable for the continual development of LEDs that demand triplet-light-energy harvesting and the large triplet emission yield, and favourable radiative decay rate of triplet excitons is beneficial.

Experimental Section

General comments: All reactions were carried out under a nitrogen atmosphere with the use of standard Schlenk techniques, but no special precautions were taken to exclude oxygen during workup. Solvents were predried and distilled from appropriate drying agents. All chemicals, unless otherwise stated, were obtained from commercial sources and used as received. Preparative TLC was performed on 0.7 mm silica plates (Merck Kieselgel 60 GF_{254}) prepared in our laboratory. The compounds *trans*-[PtCl(Ph)$(PEt_3)_2$],[48] *trans*-[$PtCl_2(PBu_3)_2$],[49] and *trans*-[{−Pt-$(PBu_3)_2$C≡C(*p*-C_6H_4)C≡C−}$_n$][23e] were prepared by literature methods. Infrared spectra were recorded as CH_2Cl_2 solutions or KBr pellets on a Nicolet Magna 550 Series II FTIR spectrometer. NMR spectra were measured in appropriate solvents on a JEOL EX 270 or a Varian INOVA 400 MHz FT-NMR spectrometer, with ^{1}H NMR chemical shifts quoted relative to $SiMe_4$ and ^{31}P chemical shifts relative to an 85 % H_3PO_4 external standard. Fast atom bombardment (FAB) mass spectra were recorded on a Finnigan MAT SSQ 710 mass spectrometer. Electronic absorption spectra were obtained with a Hewlett–Packard 8453 UV-visible spectrometer. For emission spectral measurement, the 325 nm line of a He/Cd laser was used as an excitation source. The luminescence spectra were analyzed by a 0.25 m focal-length double monochromator with a Peltier-cooled photomultiplier tube and processed with a lock-in amplifier. For low-temperature measurements, samples were mounted in a closed-cycle cryostat (Oxford CC 1104) in which the temperature could be adjusted from 10 to 330 K. The solution emission spectra were measured on a PTI Fluorescence Master Series QM 1 spectrophotometer. The fluorescence quantum yields were determined in CH_2Cl_2 solutions at 290 K against the anthracene standard ($\phi_F = 0.27$). Phosphorescence quantum yields were measured in solid thin films at 20 K relative to the prototype polymer $[Pt\text{-}T(P)T]_\infty$ ($\phi_P = 0.30$ at 20 K).[23a] The molecular weights of the polymers were determined by GPC (HP 1050 series HPLC with visible wavelength and fluorescence detectors) using polystyrene standards and thermal analyses were performed with the Perkin–Elmer TGA 6 and Pyris Diamond DSC thermal analysers at a heating rate of 20 °C min^{-1}.

Caution: Organomercurials are extremely toxic and all experimentation involving these reagents should be carried out in a well-ventilated hood.

H-T(O)T: This compound was prepared as described previously[50] and it was isolated in 88 % yield. ^{1}H NMR (270 MHz, $CDCl_3$, 25 °C, TMS): δ = 7.50 (d, ^3J(H,H) = 8.8 Hz, 4H; Ar), 6.98 (d, ^3J(H,H) = 8.8 Hz, 4H; Ar), 3.10 ppm (s, 2H; C≡CH); ^{13}C NMR (67.8 MHz, $CDCl_3$, 25 °C, TMS): δ = 156.85, 133.77, 118.77, 117.20 (Ar), 82.94, 76.92 ppm (C≡C); IR (CH_2Cl_2): $\tilde{\nu}$ = 3295 (≡CH), 2109 cm^{-1} (C≡C); FAB-MS: *m*/*z*: 218 $[M]^+$.

H-T(S)T: The synthesis followed the reported procedures with an overall yield of 41 %.[51] ^{1}H NMR (270 MHz, $CDCl_3$, 25 °C, TMS): δ = 7.43 (d, ^3J-(H,H) = 8.4 Hz, 4H; Ar), 7.28 (d, ^3J(H,H) = 8.4 Hz, 4H; Ar), 3.12 ppm (s, 2H; C≡CH); ^{13}C NMR (67.8 MHz, $CDCl_3$, 25 °C, TMS): δ = 136.31, 132.87, 130.71, 121.04 (Ar), 82.97, 78.22 ppm (C≡C); IR (CH_2Cl_2): $\tilde{\nu}$ = 3296 (≡CH), 2109 cm^{-1} (C≡C); FAB-MS: *m*/*z*: 234 $[M]^+$.

H-T(SO)T: H_2O_2(aq) (19.8 mmol, 30 %) was added to a solution of bis-(ethynylphenyl) sulfide (216 mg, 0.92 mmol) in $CHCl_3$ (40 mL) under reflux and the mixture was stirred overnight. After extraction with $CHCl_3$ and drying over $MgSO_4$, the product (160 mg, 65 %) was obtained by purification using silica gel chromatography eluting with CH_2Cl_2. ^{1}H NMR (270 MHz, $CDCl_3$, 25 °C, TMS): δ = 7.61–7.27 (m, 8H; Ar), 3.18 ppm (s, 2H; C≡CH); ^{13}C NMR (67.8 MHz, $CDCl_3$, 25 °C, TMS): δ = 145.61, 133.05, 125.32, 124.60 (Ar), 82.24, 79.65 ppm (C≡C); IR (KBr): $\tilde{\nu}$ = 3308 (≡CH), 2112 (C≡C), 1049 cm^{-1} (S=O); FAB-MS: *m*/*z*: 251 $[M]^+$; elemental analysis calcd (%) for $C_{16}H_{10}OS$: C 76.77, H 4.03; found: C 76.50, H 3.98.

H-T(SO$_2$)T: *m*CPBA (880 mg, 3.84 mmol) was added to a solution of bis(ethynylphenyl) sulfide (180 mg, 0.77 mmol) in CH_2Cl_2 (20 mL) and the mixture was stirred overnight. After extraction with CH_2Cl_2 and drying over $MgSO_4$, the product (120 mg, 57%) was isolated following silica gel chromatography by elution with CH_2Cl_2. ^{1}H NMR (270 MHz, $CDCl_3$, 25°C, TMS): $\delta = 7.88$ (d, ^3J(H,H) = 8.6 Hz, 4H; Ar), 7.59 (d, ^3J(H,H) = 8.6 Hz, 4H; Ar), 3.25 ppm (s, 2H; C≡CH); ^{13}C NMR (67.8 MHz, $CDCl_3$, 25°C, TMS): $\delta = 141.00$, 132.92, 127.64 (Ar), 81.76, 81.22 ppm (C≡C); IR (KBr): $\tilde{\nu} = 3274$ (≡CH), 2115 (C≡C), 1313, 1153 cm^{-1} (SO_2); FAB-MS: *m*/*z*: 267 $[M]^+$; elemental analysis calcd (%) for $C_{16}H_{10}O_2S$: C 72.16, H 3.78; found: C 72.03, H 3.58.

[Pt-T(O)T]: CuI (3 mg) was added to a stirred mixture of H-T(O)T (12 mg, 0.06 mmol) and *trans*-[PtCl(Ph)(PEt_3)$_2$] (60 mg, 0.11 mmol) in *i*Pr_2NH (10 mL) and CH_2Cl_2 (10 mL). The solution was stirred at room temperature (RT) over a period of 15 h, after which all volatile components were removed under vacuum. The crude product was taken up in CH_2Cl_2 and purified on preparative silica TLC plates using *n*-hexane/CH_2Cl_2 (3:2 v/v) as eluent. From the third pale yellow band ($R_f = 0.45$) we obtained [Pt-T(O)T] as a yellow solid (33 mg, 48%). ^{1}H NMR (400 MHz, $CDCl_3$, 25°C, TMS): $\delta = 7.34$–7.24 (m, 8H; Ar), 6.99–6.79 (m, 10H; Ar), 1.79–1.73 (m, 24H; CH_2 of Et), 1.14–1.05 ppm (m, 36H; CH_3 of Et); ^{13}C NMR (100.3 MHz, $CDCl_3$, 25°C, TMS): $\delta = 156.44$, 154.52, 139.15, 132.01, 127.25, 124.32, 121.15, 118.37 (Ar), 111.64, 109.26 (C≡C), 15.01, 8.01 ppm (Et); ^{31}P NMR (161.9 MHz, $CDCl_3$, 25°C, 85% H_3PO_4): $\delta = 10.89$ ppm (^1J(Pt,P) = 2641 Hz); IR (CH_2Cl_2): $\tilde{\nu} = 2097$ cm^{-1} (C≡C); FAB-MS: *m*/*z*: 1232 $[M]^+$; elemental analysis calcd (%) for $C_{52}H_{78}OP_4Pt_2$: C 50.64, H 6.37; found: C 50.32, H 6.08.

[Pt-T(S)T]: The procedure used to synthesise this compound was similar to that used for [Pt-T(O)T] except that H-T(S)T (22 mg, 0.09 mmol) was used instead of H-T(O)T. [Pt-T(S)T] was obtained as a yellow solid (60 mg, 52%) after column chromatography eluting with *n*-hexane/CH_2Cl_2 (3:1 v/v). ^{1}H NMR (400 MHz, $CDCl_3$, 25°C, TMS): $\delta = 7.33$–7.15 (m, 12H; Ar), 6.96 (m, 4H; Ar), 6.80 (m, 2H; Ar), 1.78–1.71 (m, 24H; CH_2 of Et), 1.13–1.05 ppm (m, 36H; CH_3 of Et); ^{13}C NMR (100.3 MHz, $CDCl_3$, 25°C, TMS): $\delta = 156.20$, 139.08, 131.53, 131.44, 130.62, 128.13, 127.26, 121.21 (Ar), 114.93, 109.67 (C≡C), 15.21, 8.10 ppm (Et); ^{31}P NMR (161.9 MHz, $CDCl_3$, 25°C, 85% H_3PO_4): $\delta = 10.95$ ppm (^1J(Pt,P) = 2636 Hz); IR (CH_2Cl_2): $\tilde{\nu} = 2094$ cm^{-1} (C≡C); FAB-MS: *m*/*z*: 1248 $[M]^+$; elemental analysis calcd (%) for $C_{52}H_{78}P_4Pt_2S$: C 49.99, H 6.29; found: C 49.78, H 6.02.

[Pt-T(SO)T]: The procedure used to synthesise this compound was similar to that used for [Pt-T(O)T] except that H-T(SO)T (14 mg, 0.06 mmol) was used and [Pt-T(SO)T] was obtained as a yellow solid (42 mg, 60%) after column chromatography eluting with *n*-hexane/CH_2Cl_2 (4:1 v/v). ^{1}H NMR (400 MHz, $CDCl_3$, 25°C, TMS): $\delta = 7.45$–7.26 (m, 12H; Ar), 6.96 (m, 4H; Ar), 6.80 (m, 2H; Ar), 1.74–1.69 (m, 24H; CH_2 of Et), 1.14–1.02 ppm (m, 36H; CH_3 of Et); ^{13}C NMR (100.3 MHz, $CDCl_3$, 25°C, TMS): $\delta = 155.89$, 140.65, 139.00, 131.41, 128.33, 127.33, 124.67, 121.32 (Ar), 109.72, 108.13 (C≡C), 15.01, 7.97 ppm (Et); ^{31}P NMR (161.9 MHz, $CDCl_3$, 25°C, 85% H_3PO_4): $\delta = 11.01$ ppm (^1J(Pt,P) = 2630 Hz); IR (KBr): $\tilde{\nu} = 2093$ (C≡C), 1040 cm^{-1} (S=O); FAB-MS: *m*/*z*: 1265 $[M]^+$; elemental analysis calcd (%) for $C_{52}H_{78}OP_4Pt_2S$: C 49.36, H 6.21; found: C 49.12, H 5.98.

[Pt-T(SO$_2$)T]: Similar to the preparation of [Pt-T(O)T], H-T(SO$_2$)T (15 mg, 0.06 mmol) was used to give [Pt-T(SO$_2$)T] as a yellow solid (40 mg, 57%) after column chromatography using *n*-hexane/CH_2Cl_2 (4:1 v/v) as eluent. ^{1}H NMR (400 MHz, $CDCl_3$, 25°C, TMS): $\delta = 7.72$ (m, 4H; Ar), 7.32–7.28 (m, 8H; Ar), 6.96 (m, 4H; Ar), 6.80 (m, 2H; Ar), 1.76–1.66 (m, 24H; CH_2 of Et), 1.14–1.02 ppm (m, 36H; CH_3 of Et); ^{13}C NMR (100.3 MHz, $CDCl_3$, 25°C, TMS): $\delta = 138.93$, 136.86, 134.36, 131.12, 130.93, 128.82, 127.39, 127.17 (Ar), 121.41, 109.88 (C≡C), 15.00, 7.97 ppm (Et); ^{31}P NMR (161.9 MHz, $CDCl_3$, 25°C, 85% H_3PO_4): $\delta = 11.03$ ppm (^1J(Pt,P) = 2614 Hz); IR (KBr): $\tilde{\nu} = 2090$ (C≡C), 1371, 1155 cm^{-1} (SO_2); FAB-MS: *m*/*z*: 1281 $[M]^+$; elemental analysis calcd (%) for $C_{52}H_{78}O_2P_4Pt_2S$: C 48.74, H 6.14; found: C 48.55, H 6.00.

[Pt-T(O)T]$_\infty$: Polymerization was carried out by mixing H-T(O)T (26 mg, 0.12 mmol), *trans*-[$PtCl_2$(PBu_3)$_2$] (80 mg, 0.12 mmol), and CuI (3 mg) in *i*Pr_2NH/CH_2Cl_2 (20 mL, 1:1 v/v). After stirring at RT for 15 h, the solution mixture was evaporated to dryness. The residue was redissolved in CH_2Cl_2, and filtered through a silica column using the same eluent to remove ionic impurities and catalyst residues. After removal of the solvent, the crude product was purified by precipitation in toluene from MeOH. Subsequent washing with *n*-hexane and drying in vacuo gave [Pt-T(O)T]$_\infty$ as a yellow powder (69 mg, 71%). ^{1}H NMR (400 MHz, $CDCl_3$, 25°C, TMS): $\delta = 7.26$–7.19 (m, 4H; Ar), 6.84 (m, 4H; Ar), 2.15–2.11 (m, 12H; PCH_2), 1.60–1.57 (m, 12H; PCH_2CH_2), 1.47–1.41 (m, 12H; CH_2CH_3), 0.92 ppm (t, ^3J(H,H) = 7.2 Hz, 18H; CH_3); ^{13}C NMR (100.3 MHz, $CDCl_3$, 25°C, TMS): $\delta = 154.66$, 131.93, 124.07, 118.39 (Ar), 107.99, 106.83 (C≡C), 26.32, 24.41, 23.83, 13.83 ppm (Bu); ^{31}P NMR (161.9 MHz, $CDCl_3$, 25°C, 85% H_3PO_4): $\delta = 3.96$ ppm (^1J(Pt,P) = 2357 Hz); IR (CH_2Cl_2): $\tilde{\nu} = 2102$ cm^{-1} (C≡C); elemental analysis calcd (%) for $(C_{40}H_{62}OP_2Pt)_n$: C 58.88, H 7.66; found: C 58.58, H 7.43.

[Pt-T(S)T]$_\infty$: This polymer was prepared by using a similar procedure to that desribed above for [Pt-T(O)T]$_\infty$ by using H-T(S)T (35 mg, 0.15 mmol) and *trans*-[$PtCl_2$(PBu_3)$_2$] (100 mg, 0.15 mmol) to give [Pt-T(S)T]$_\infty$ as a yellow powder (50 mg, 40%). ^{1}H NMR (400 MHz, $CDCl_3$, 25°C, TMS): $\delta = 7.24$–7.13 (m, 8H; Ar), 2.12–2.08 (m, 12H; PCH_2), 1.57–1.56 (m, 12H; PCH_2CH_2), 1.46–1.39 (m, 12H; CH_2CH_3), 0.92–0.88 ppm (m, 18H; CH_3); ^{13}C NMR (100.3 MHz, $CDCl_3$, 25°C, TMS): $\delta = 131.85$, 131.35, 130.58, 127.75 (Ar), 109.75, 108.54 (C≡C), 26.30, 24.21, 23.67, 13.77 ppm (Bu); ^{31}P NMR (161.9 MHz, $CDCl_3$, 25°C, 85% H_3PO_4): $\delta = 4.10$ ppm (^1J(Pt,P) = 2350 Hz); IR (CH_2Cl_2): $\tilde{\nu} = 2099$ cm^{-1} (C≡C); elemental analysis calcd (%) for $(C_{40}H_{62}P_2PtS)_n$: C 57.74, H 7.51; found: C 57.42, H 7.23.

[Pt-T(SO)T]$_\infty$: Following the same synthetic approach described for [Pt-T(O)T]$_\infty$, a yellow solid of [Pt-T(SO)T]$_\infty$ (60 mg, 79%) was obtained using H-T(SO)T (30 mg, 0.12 mmol) and *trans*-[$PtCl_2$(PBu_3)$_2$] (80 mg, 0.12 mmol). ^{1}H NMR (400 MHz, $CDCl_3$, 25°C, TMS): $\delta = 7.44$ (d, ^3J(H,H) = 8.4 Hz, 4H; Ar), 7.28 (d, ^3J(H,H) = 8.4 Hz, 4H; Ar), 2.08–2.05 (m, 12H; PCH_2), 1.57–1.55 (m, 12H; PCH_2CH_2), 1.47–1.37 (m, 12H; CH_2CH_3), 0.89 ppm (t, ^3J(H,H) = 7.2 Hz, 18H; CH_3); ^{13}C NMR (100.3 MHz, $CDCl_3$, 25°C, TMS): $\delta = 140.95$, 131.81, 131.27, 124.75 (Ar), 112.78, 108.63 (C≡C), 26.25, 24.31, 23.81, 13.74 ppm (Bu); ^{31}P NMR (161.9 MHz, $CDCl_3$, 25°C, 85% H_3PO_4): $\delta = 4.85$ ppm (^1J(Pt,P) = 2326 Hz); IR (KBr): $\tilde{\nu} = 2098$ (C≡C), 1043 cm^{-1} (S=O); elemental analysis calcd (%) for $(C_{40}H_{62}OP_2PtS)_n$: C 56.65, H 7.37; found: C 56.44, H 7.05.

[Pt-T(SO$_2$)T]$_\infty$: A procedure similar to that described above for [Pt-T(O)T]$_\infty$ was used to obtain the [Pt-T(SO$_2$)T]$_\infty$ (83 mg, 81%) from H-T(SO$_2$)T (32 mg, 0.12 mmol) and *trans*-[$PtCl_2$(PBu_3)$_2$] (80 mg, 0.12 mmol). ^{1}H NMR (400 MHz, $CDCl_3$, 25°C, TMS): $\delta = 7.74$ (d, ^3J(H,H) = 8.4 Hz, 4H; Ar), 7.28 (d, ^3J(H,H) = 8.4 Hz, 4H; Ar), 2.08–2.04 (m, 12H; PCH_2), 1.56–1.53 (m, 12H; PCH_2CH_2), 1.45–1.36 (m, 12H; CH_2CH_3), 0.89 ppm (m, 18H; CH_3); ^{13}C NMR (100.3 MHz, $CDCl_3$, 25°C, TMS): $\delta = 137.22$, 133.81, 130.99, 127.22 (Ar), 115.66, 108.79 (C≡C), 26.24, 24.30, 23.81, 13.73 ppm (Bu); ^{31}P NMR (161.9 MHz, $CDCl_3$, 25°C, 85% H_3PO_4): $\delta = 4.45$ ppm (^1J(Pt,P) = 2319 Hz); IR (KBr): $\tilde{\nu} = 2097$ (C≡C), 1317, 1151 cm^{-1} (SO_2); elemental analysis calcd (%) for $(C_{40}H_{62}O_2P_2PtS)_n$: C 55.61, H 7.23; found: C 55.39, H 7.33.

[Au-T(O)T]: Au(PPh_3)Cl (25 mg 0.05 mmol) in MeOH (15 mL) was mixed with H-T(O)T (4.6 mg, 0.02 mmol) in CH_2Cl_2 (5 mL). NaOMe (0.3 mL, 0.35 mmol) was added to this solution. Within a few minutes, a light yellow solid precipitated from the homogeneous solution. The solid was then collected by filtration after stirring for 2 h, was washed with MeOH and was air-dried to give [Au-T(O)T] (16 mg, 67%). ^{1}H NMR (400 MHz, $CDCl_3$, 25°C, TMS): $\delta = 7.58$–7.43 (m, 34H; Ar), 6.89 ppm (m, 4H; Ar); ^{13}C NMR (100.3 MHz, $CDCl_3$, 25°C, TMS): $\delta = 155.82$, 134.37, 133.81, 131.53, 129.99, 129.44, 129.17, 118.49 (Ar), 103.77, 103.50 ppm (C≡C); ^{31}P NMR (161.9 MHz, $CDCl_3$, 25°C, 85% H_3PO_4): $\delta = 43.38$ ppm; IR (CH_2Cl_2): $\tilde{\nu} = 2112$ cm^{-1} (C≡C); FAB-MS: *m*/*z*: 1134 $[M]^+$; elemental analysis calcd (%) for $C_{52}H_{38}Au_2OP_2$: C 55.04, H 3.38; found: C 54.86, H 3.40.

[Au-T(S)T]: This complex was prepared by using the same conditions as described above for [Au-T(O)T], but H-T(S)T (4.9 mg, 0.02 mmol) was used instead to produce a light yellow solid in 54% yield (13 mg). ^{1}H NMR (400 MHz, $CDCl_3$, 25°C, TMS): $\delta = 7.58$–7.41 (m, 32H; Ar),

7.21–7.19 (m, 4H; Ar), 7.06 ppm (m, 2H; Ar); ^{13}C NMR (100.3 MHz, $CDCl_3$, 25 °C, TMS): δ = 134.36, 134.22, 133.01, 131.56, 130.46, 129.94, 129.18, 129.07 (Ar), 103.83, 103.51 ppm (C≡C); ^{31}P NMR (161.9 MHz, $CDCl_3$, 25 °C, 85% H_3PO_4): δ = 43.30 ppm; IR (CH_2Cl_2): $\tilde{\nu}$ = 2117 cm^{-1} (C≡C); FAB-MS: *m*/*z*: 1150 $[M]^+$; elemental analysis calcd (%) for $C_{52}H_{38}Au_2P_2S$: C 54.27, H 3.33; found: C 54.02, H 3.10.

[Au-T(SO)T]: According to the same procedure described for the synthesis of [Au-T(O)T], [Au-T(SO)T] was isolated from H-T(SO)T (5.3 mg, 0.02 mmol) as a pale yellow solid in 61% yield (15 mg). ^{1}H NMR (400 MHz, $CDCl_3$, 25 °C, TMS): δ = 7.57–7.27 ppm (m, 38H; Ar); ^{13}C NMR (100.3 MHz, $CDCl_3$, 25 °C, TMS): δ = 142.99, 134.19, 133.03, 131.58, 129.80, 129.09, 128.06, 124.78 (Ar), 103.01, 102.86 ppm (C≡C); ^{31}P NMR (161.9 MHz, $CDCl_3$, 25 °C, 85% H_3PO_4): δ = 43.14 ppm; IR (KBr): $\tilde{\nu}$ = 2116 (C≡C), 1043 cm^{-1} (S=O); FAB-MS: *m*/*z*: 1166 $[M]^+$; elemental analysis calcd (%) for $C_{52}H_{38}Au_2OP_2S$: C 53.53, H 3.28; found: C 53.45, H 3.06.

[Au-T(SO$_2$)T]: This compound was synthesised by a similar procedure to that for [Au-T(O)T] from H-T(SO$_2$)T (5.4 mg, 0.02 mmol), and it was isolated as a pale yellow solid in 85% yield (20 mg). ^{1}H NMR (400 MHz, $CDCl_3$, 25 °C, TMS): δ = 7.79 (m, 4H; Ar), 7.58–7.44 ppm (m, 34H; Ar); ^{13}C NMR (100.3 MHz, $CDCl_3$, 25 °C, TMS): δ = 138.92, 134.18, 132.82, 131.65, 130.37, 129.71, 129.12, 127.33 (Ar), 102.44, 102.56 ppm (C≡C); ^{31}P NMR (161.9 MHz, $CDCl_3$, 25 °C, 85% H_3PO_4): δ = 42.99 ppm; IR (KBr): $\tilde{\nu}$ = 2115 (C≡C), 1317, 1154 cm^{-1} (SO_2); FAB-MS: *m*/*z*: 1182 $[M]^+$; elemental analysis calcd (%) for $C_{52}H_{38}Au_2O_2P_2S$: C 52.80, H 3.24; found: C 52.55, H 3.03.

[Hg-T(O)T]: The organic diyne H-T(O)T (16 mg, 0.08 mmol) in MeOH (10 mL) was first combined with MeHgCl (50 mg, 0.20 mmol) in MeOH (10 mL). We subsequently added 0.20 M basic MeOH (13 mL) to give a pale yellow suspension. The solvent was then decanted and the light yellow solid of [Hg-T(O)T] was washed with MeOH (2×20 mL) and air-dried (19 mg, 41%). ^{1}H NMR (400 MHz, $CDCl_3$, 25 °C, TMS): δ = 7.44 (d, ^3J(H,H) = 7.0 Hz, 4H; Ar), 6.93 (d, ^3J(H,H) = 7.0 Hz, 4H; Ar), 0.69 ppm (t, ^3J(H,H) = 140 Hz, 6H; HgMe); ^{13}C NMR (100.3 MHz, $CDCl_3$, 25 °C, TMS): δ = 156.42, 142.24, 133.67, 118.76 (Ar), 118.31, 104.62 (C≡C), 7.26 ppm (Me); IR (CH_2Cl_2): $\tilde{\nu}$ = 2138 cm^{-1} (C≡C); FAB-MS: *m*/*z*: 647 $[M]^+$; elemental analysis calcd (%) for $C_{18}H_{14}Hg_2O$: C 33.39, H 2.18; found: C 33.13, H 2.05.

[Hg-T(S)T]: Similar to [Hg-T(O)T], [Hg-T(S)T] was prepared from H-T(S)T (20 mg, 0.08 mmol) and collected as a light yellow solid with a yield of 71% (40 mg). ^{1}H NMR (400 MHz, $CDCl_3$, 25 °C, TMS): δ = 7.39 (d, ^3J(H,H) = 7.6 Hz, 4H; Ar), 7.35 (m, 4H; Ar), 0.70 ppm (t, ^3J(H,H) = 146 Hz, 6H; HgMe); ^{13}C NMR (100.3 MHz, $CDCl_3$, 25 °C, TMS): δ = 144.21, 135.40, 132.81, 130.70 (Ar), 122.05, 104.59 (C≡C), 7.11 ppm (Me); IR (CH_2Cl_2): $\tilde{\nu}$ = 2135 cm^{-1} (C≡C); FAB-MS: *m*/*z*: 663 $[M]^+$; elemental analysis calcd (%) for $C_{18}H_{14}Hg_2S$: C 32.58, H 2.13; found: C 32.33, H 2.05.

[Hg-T(SO)T]: A procedure similar to that employed for [Hg-T(O)T] was used to give [Hg-T(SO)T] as a light yellow powder in 43% yield (24 mg) from H-T(SO)T (20 mg, 0.08 mmol). ^{1}H NMR (400 MHz, $CDCl_3$, 25 °C, TMS): δ = 7.56–7.50 (m, 8H; Ar), 0.71 ppm (t, ^3J(H,H) = 142 Hz, 6H; HgMe); ^{13}C NMR (100.3 MHz, $CDCl_3$, 25 °C, TMS): δ = 146.25, 144.57, 132.94, 124.71 (Ar), 126.50, 103.80 (C≡C), 7.09 ppm (Me); IR (KBr): $\tilde{\nu}$ = 2115 (C≡C), 1043 cm^{-1} (S=O); FAB-MS: *m*/*z*: 680 $[M]^+$; elemental analysis calcd (%) for $C_{18}H_{14}Hg_2OS$: C 31.81, H 2.08; found: C 31.68, H 1.96.

[Hg-T(SO$_2$)T]: By using H-T(SO$_2$)T (20 mg, 0.07 mmol), an off-white solid of [Hg-T(SO$_2$)T] was collected (30 mg, 58%) after the usual workup. ^{1}H NMR (400 MHz, $CDCl_3$, 25 °C, TMS): δ = 7.84 (d, ^3J(H,H) = 7.6 Hz, 4H; Ar), 7.54 (d, ^3J(H,H) = 7.6 Hz, 4H; Ar), 0.73 ppm (t, ^3J(H,H) = 148 Hz, 6H; HgMe); ^{13}C NMR (100.3 MHz, $CDCl_3$, 25 °C, TMS): δ = 148.36, 140.08, 132.78, 127.58 (Ar), 128.82, 103.31 (C≡C), 7.06 ppm (Me); IR (KBr): $\tilde{\nu}$ = 2137 (C≡C), 1320, 1156 cm^{-1} (SO_2); FAB-MS: *m*/*z*: 696 $[M]^+$; elemental analysis calcd (%) for $C_{18}H_{14}Hg_2O_2S$: C 31.08, H 2.03; found: C 30.89, H 1.94.

Crystallography: Single crystals of seven compounds suitable for X-ray crystallographic analyses were grown by slow evaporation of their respective solutions in CH_2Cl_2/*n*-hexane at RT. Crystal data, data collection parameters, and refinement results are listed in Table 7. The diffraction experiments were carried out at 293 K on a Bruker Axs SMART1000 CCD area-detector diffractometer using graphite-monochromated $Mo_{K\alpha}$ radiation (λ = 0.71073 Å). The raw intensity data frames were integrated with the SAINT+ program using a narrow-frame integration algorithm.[52] Corrections for Lorentz and polarization effects were also applied by

Table 7. Summary of crystal structure data.

	[Pt-T(S)T]	[Pt-T(SO)T]	[Pt-T(SO$_2$)T]	[Au-T(O)T]	[Hg-T(S)T]	[Hg-T(SO)T]	[Hg-T(SO$_2$)T]
formula	$C_{52}H_{78}P_4S$	$C_{52}H_{78}OP_4Pt_2S$	$C_{52}H_{78}O_2P_4Pt_2S$	$C_{58}H_{52}Au_2OP_2$	$C_{18}H_{14}Hg_2S$	$C_{18}H_{14}Hg_2OS$	$C_{18}H_{14}Hg_2O_2S$
M_r	1249.26	1265.26	1281.26	1220.87	663.53	679.53	695.53
crystal size [mm^3]	0.34×0.25×0.24	0.30×0.22×0.20	0.30×0.25×0.22	0.28×0.18×0.15	0.20×0.15×0.10	0.22×0.12×0.08	0.20×0.15× 0.09
crystal system	triclinic	monoclinic	monoclinic	monoclinic	monoclinic	triclinic	triclinic
space group	$P\bar{1}$	*C*2/*c*	*C*2/*c*	$P2_1$/n	*C*2/*c*	$P\bar{1}$	$P\bar{1}$
a [Å]	9.7257(19)	30.527(2)	30.2194(14)	10.8149(9)	20.3521(15)	4.6555(5)	5.1002(8)
b [Å]	14.376(3)	9.0077(6)	9.0729(4)	12.9381(12)	7.6683(6)	13.5283(15)	8.2840(13)
c [Å]	40.030(8)	20.4816(13)	20.6748(10)	37.132(3)	23.2552(17)	14.9441(16)	21.458(3)
α [°]	89.89(3)	90	90	90	90	65.360(2)	100.238(3)
β [°]	89.94(3)	92.5040(10)	92.6350(10)	98.281(2)	106.0430(10)	89.928(2)	91.990(3)
γ [°]	84.45(3)	90	90	90	90	82.482(2)	101.242(3)
V [Å^3]	5570.7(19)	5626.7(6)	5662.6(5)	5141.5(8)	3488.0(5)	846.66(16)	872.8(2)
Z	4	4	4	4	8	2	2
ρ_{calcd} [g cm^{-3}]	1.490	1.494	1.503	1.577	2.527	2.666	2.647
μ [mm^{-1}]	5.200	5.151	5.120	5.800	17.694	18.232	17.693
F(000)	2488	2520	2552	2384	2384	612	628
θ range [°]	1.42–25.00	1.99–25.00	1.97–25.00	1.93–28.31	1.82–25.00	2.76–24.99	1.93–25.00
reflns collected	55186	13465	13678	30444	7844	3433	4276
unique reflns	19583	4958	4974	11954	3049	2605	2973
R_{int}	0.0560	0.0298	0.0368	0.0573	0.0650	0.0448	0.0383
reflns obsvd [$I > 2.0\sigma(I)$]	11860	3806	4102	6429	2257	2062	2318
parameters	1063	276	276	538	191	200	209
*R*1, *wR*2 [$I > 2.0\sigma(I)$][a]	0.0433, 0.0745	0.0338, 0.0805	0.0276, 0.0677	0.0455, 0.0968	0.0494, 0.1264	0.0644, 0.1559	0.0485, 0.1361
*R*1, *wR*2 (all data)	0.0887, 0.0841	0.0499, 0.0893	0.0380, 0.0737	0.1119, 0.1210	0.0681, 0.1453	0.0735, 0.1621	0.0625, 0.1555
GoF on F^2[b]	0.876	1.021	1.018	0.949	0.913	0.989	0.947

[a] $R1 = \Sigma\,||F_o| - |F_c||/\Sigma|F_o|$. $wR2 = \{\Sigma[w(F_o^2 - F_c^2)^2]/\Sigma[w(F_o^2)^2]\}^{1/2}$. [b] $GoF = [(\Sigma w\,||F_o| - |F_c||)^2/(N_{obs} - N_{param})]^{1/2}$.

SAINT. For each analysis, an empirical absorption correction based on the multiple measurement of equivalent reflections was applied by using the program SADABS.[53] The structures were solved by direct methods, and expanded by difference Fourier syntheses using the software SHELTXL.[54] Structure refinements were made on F^2 by the full-matrix least-squares technique. Unless stated otherwise, all the non-hydrogen atoms were refined with anisotropic displacement parameters. The hydrogen atoms were placed in their ideal positions, but were not refined.

CCDC-280336 ([Pt-T(S)T]), CCDC-280337 ([Pt-T(SO)T]), CCDC-280338 ([Pt-T(SO_2)T]), CCDC-280339 ([Au-T(O)T]), CCDC-280340 ([Hg-T(S)T]), CCDC-280341 ([Hg-T(SO)T]), and CCDC-280342 ([Hg-T-(SO_2)T]) contain the supplementary crystallographic data for this paper. These data can be obtained free of charge from the Cambridge Crystallographic Data Centre via www.ccdc.cam.ac.uk/data_request/cif.

Acknowledgements

Financial support from a CERG Grant from the Research Grants Council of the Hong Kong SAR, P.R. China (Project No. HKBU 2054/02P) is gratefully acknowledged for this work. S.-Y.P. acknowledges the receipt of a Li Po Chun Charitable Trust Fund Postgraduate Scholarship, administered by Hong Kong Baptist University. We also thank Dr. Z. Lin for helpful discussions.

[1] *Conjugated Polymeric Materials: Opportunities in Electronics, Optoelectronics, and Molecular Electronics* (Eds.: J. L. Brédas, R. R. Chance), Kluwer Academic, Dordrecht, **1990**.
[2] R. E. Martin, F. Diederich, *Angew. Chem.* **1999**, *111*, 1440; *Angew. Chem. Int. Ed.* **1999**, *38*, 1350.
[3] P. J. Stang, F. Diederich, *Modern Acetylene Chemistry*, Wiley-VCH, Weinheim, Germany, **1995**.
[4] F. Diederich, *Chem. Commun.* **2001**, 219.
[5] U. H. F. Bunz, *Chem. Rev.* **2000**, *100*, 1605.
[6] J. M. Tour, *Acc. Chem. Res.* **2000**, *33*, 791.
[7] a) N. J. Long, C. K. Williams, *Angew. Chem.* **2003**, *115*, 2690; *Angew. Chem. Int. Ed.* **2003**, *42*, 2586; b) W.-Y. Wong, *J. Inorg. Organomet. Polym. Mater.* **2005**, *15*, 197; c) W.-Y. Wong, *Comments Inorg. Chem.* **2005**, *26*, 39.
[8] a) P. Nguyen, P. Gómez-Elipe, I. Manners, *Chem. Rev.* **1999**, *99*, 1515; b) I. Manners, *Synthetic Metal-Containing Polymers*, Wiley-VCH, Weinheim, **2004**, Chapter 5, p. 153; c) V. W.-W. Yam, *Acc. Chem. Res.* **2002**, *35*, 555.
[9] J. L. Brédas, J. Cornil, A. J. Heeger, *Adv. Mater.* **1996**, *8*, 447.
[10] *Primary Photoexcitations in Conjugated Polymers: Molecular Exciton vs Semiconductor Band Model* (Ed.: N. S. Sariciftci), World Scientific, Singapore, **1997**.
[11] *Handbook of Conducting Polymers* (Eds.: T. A. Skotheim, J. R. Reynolds, R. L. Elsenbaumer), Marcel Dekker, New York, 2nd ed., **1998**.
[12] P. K. H. Ho, J. S. Kim, J. H. Burroughes, H. Becker, S. F. Y. Li, T. M. Brown, F. Cacialli, R. H. Friend, *Nature* **2000**, *404*, 481.
[13] Y. Cao, I. D. Parker, G. Yu, C. Zhang, A. J. Heeger, *Nature* **1999**, *397*, 414.
[14] M. A. Baldo, D. F. O'Brien, Y. You, A. Shoustikov, S. Sibley, M. E. Thompson, S. R. Forrest, *Nature* **1998**, *395*, 151.
[15] M. A. Baldo, M. E. Thompson, S. R. Forrest, *Nature* **2000**, *403*, 750.
[16] R. H. Friend, R. W. Gymer, A. B. Holmes, J. H. Burroughes, R. N. Marks, C. Taliani, D. D. C. Bradley, D. A. Dos Santos, J. L. Brédas, M. Lögdlund, W. R. Salaneck, *Nature* **1999**, *397*, 121.
[17] J. S. Wilson, A. S. Dhoot, A. J. A. B. Seeley, M. S. Khan, A. Köhler, R. H. Friend, *Nature* **2001**, *413*, 828.
[18] A. Köhler, J. S. Wilson, R. H. Friend, *Adv. Mater.* **2002**, *14*, 701.
[19] C. Adachi, M. A. Baldo, M. E. Thompson, S. R. Forrest, *J. Appl. Phys.* **2001**, *90*, 5048.
[20] J. M. Lupton, A. Pogantsch, T. Piok, E. J. W. List, S. Patil, U. Scherf, *Phys. Rev. Lett.* **2002**, *89*, 167401.
[21] Y. V. Romanovskii, A. Gerhard, B. Schweitzer, U. Scherf, R. I. Personov, H. Bässler, *Phys. Rev. Lett.* **2000**, *84*, 1027.
[22] A. S. Dhoot, N. C. Greenham, *Adv. Mater.* **2002**, *14*, 1834.
[23] a) J. S. Wilson, N. Chawdhury, M. R. A. Al-Mandhary, M. Younus, M. S. Khan, P. R. Raithby, A. Köhler, R. H. Friend, *J. Am. Chem. Soc.* **2001**, *123*, 9412; b) M. S. Khan, M. R. A. Al-Mandhary, M. K. Al-Suti, B. Ahrens, M. F. Mahon, L. Male, P. R. Raithby, C. E. Boothby, A. Köhler, *Dalton Trans.* **2003**, 74; c) M. S. Khan, M. R. A. Al-Mandhary, M. K. Al-Suti, A. K. Hisahm, P. R. Raithby, B. Ahrens, M. F. Mahon, L. Male, E. A. Marseglia, E. Tedesco, R. H. Friend, A. Köhler, N. Feeder, S. J. Teat, *J. Chem. Soc. Dalton Trans.* **2002**, 1358; d) J. S. Wilson, A. Köhler, R. H. Friend, M. K. Al-Suti, M. R. A. Al-Mandhary, M. S. Khan, P. R. Raithby, *J. Chem. Phys.* **2000**, *113*, 7627; e) N. Chawdhury, A. Köhler, R. H. Friend, M. Younus, N. J. Long, P. R. Raithby, J. Lewis, *Macromolecules* **1998**, *31*, 722; f) N. Chawdhury, A. Köhler, R. H. Friend, W.-Y. Wong, J. Lewis, M. Younus, P. R. Raithby, T. C. Corcoran, M. R. A. Al-Mandhary, M. S. Khan, *J. Chem. Phys.* **1999**, *110*, 4963.
[24] a) W.-Y. Wong, C.-K. Wong, G.-L. Lu, A. W.-M. Lee, K.-W. Cheah, J.-X. Shi, *Macromolecules* **2003**, *36*, 983; b) W.-Y. Wong, G.-L. Lu, K.-H. Choi, J.-X. Shi, *Macromolecules* **2002**, *35*, 3506; c) W.-Y. Wong, C.-K. Wong, G.-L. Lu, K.-W. Cheah, J.-X. Shi, *J. Chem. Soc. Dalton Trans.* **2002**, 4587; d) W.-Y. Wong, S.-Y. Poon, A. W.-M. Lee, J.-X. Shi, K.-W. Cheah, *Chem. Commun.* **2004**, 2420.
[25] a) H.-Y. Chao, W. Lu, Y. Li, M. C. W. Chan, C.-M. Che, K.-K. Cheung, N. Zhu, *J. Am. Chem. Soc.* **2002**, *124*, 14696; b) W. Lu, H.-F. Xiang, N. Zhu, C.-M. Che, *Organometallics* **2002**, *21*, 2343; c) C.-M. Che, H.-Y. Chao, V. M. Miskowski, Y. Li, K.-K. Cheung, *J. Am. Chem. Soc.* **2001**, *123*, 4985.
[26] W.-Y. Wong, L. Liu, J.-X. Shi, *Angew. Chem.* **2003**, *115*, 4198; *Angew. Chem. Int. Ed.* **2003**, *42*, 4064.
[27] J. Leuninger, J. Uebe, J. Salbeck, L. Gherghel, C. S. Wang, K. Müllen, *Synth. Met.* **1999**, *100*, 79.
[28] M. A. Shahram, S. Yaghoub, H. Mehdi, A. F. Leila, *Eur. Polym. J.* **2005**, *41*, 491.
[29] J. P. Kim, W. Y. Lee, J. W. Kang, S. K. Kwon, J. J. Kim, J. S. Lee, *Macromolecules* **2001**, *34*, 7817.
[30] S. W. Hwang, Y. Chen, *Macromolecules* **2002**, *35*, 5438.
[31] W. F. Hale, A. G. Farnham, R. N. Johnson, R. A. Clendinning, *J. Polym. Sci. Part A* **1967**, *5*, 2399.
[32] R. N. Johnson, A. G. Farnham, R. A. Clendinning, W. F. Hale, C. N. Merriman, *J. Polym. Sci. Part A* **1967**, *5*, 2375.
[33] F. A. Bottino, G. D. Pasquale, L. Scalia, A. Pollicino, *Polymer* **2001**, *42*, 3323.
[34] W. S. Jenks, W. Lee, D. Shutters, *J. Phys. Chem.* **1994**, *98*, 2282, and references therein.
[35] W. Lee, W. S. Jenks, *J. Org. Chem.* **2001**, *66*, 474.
[36] a) W.-Y. Wong, K.-H. Choi, G.-L. Lu, Z. Lin, *Organometallics* **2002**, *21*, 4475; b) W.-Y. Wong, K.-H. Choi, G.-L. Lu, J.-X. Shi, P.-Y. Lai, S.-M. Chan, Z. Lin, *Organometallics* **2001**, *20*, 5446; c) B. Ahrens, K.-H. Choi, M. S. Khan, P. Li, P. R. Raithby, P. J. Wilson, W.-Y. Wong, *CrystEngComm* **2002**, *4*, 405.
[37] a) P. Pyykko, *Chem. Rev.* **1997**, *97*, 597, and references therein; b) K. R. Flower, V. J. Howard, S. Naguthney, R. G. Pritchard, J. E. Warren, A. T. McGown, *Inorg. Chem.* **2002**, *41*, 1907; c) S. S. Batsanov, *J. Chem. Soc. Dalton Trans.* **1998**, 1541.
[38] A. Bondi, *J. Phys. Chem.* **1964**, *68*, 441.
[39] S. J. Faville, W. Henderson, T. J. Mathieson, B. K. Nicholson, *J. Organomet. Chem.* **1999**, *580*, 363.
[40] X. Wang, L. Andrews, *Inorg. Chem.* **2004**, *43*, 7146.
[41] W.-Y. Wong, G.-L. Lu, L. Li, J.-X. Shi, Z. Lin, *Eur. J. Inorg. Chem.* **2004**, 2066.
[42] D. Beljonne, H. F. Wittmann, A. Köhler, S. Graham, M. Younus, J. Lewis, P. R. Raithby, M. S. Khan, R. H. Friend, J. L. Brédas, *J. Chem. Phys.* **1996**, *105*, 386.
[43] D. Hertel, S. Setayesh, H. G. Nothofer, U. Scherf, K. Müllen, H. Bässler, *Adv. Mater.* **2001**, *13*, 65.
[44] A. P. Monkman, H. D. Burrows, L. J. Hartwell, L. E. Horsburgh, I. Hamblett, S. Navaratnam, *Phys. Rev. Lett.* **2001**, *86*, 1358.

[45] S. D. Cummings, R. Eisenberg, *J. Am. Chem. Soc.* **1996**, *118*, 1949.
[46] N. J. Demas, G. A. Crosby, *J. Am. Chem. Soc.* **1970**, *92*, 7262.
[47] N. J. Turro, *Modern Molecular Photochemistry*, University Science Books, Mill Valley, CA, **1991**.
[48] G. W. Parshall, *Inorg. Synth. Vol. XII*, **1970**, p. 27.
[49] G. B. Kauffman, L. A. Teterm, *Inorg. Synth. Vol. VII*, **1963**, p. 245.
[50] B. J. L. Royles, D. M. Smith, *J. Chem. Soc. Perkin Trans. 1* **1994**, 355.
[51] E. W. Kwock, T. Baird, Jr., T. M. Miller, *Macromolecules* **1993**, *26*, 2935.
[52] SAINT+ Version 6.02a, Bruker Analytical X-ray System, Madison, WI, **1998**.
[53] G. M. Sheldrick, SADABS. Empirical Absorption Correction Program, University of Göttingen (Germany), **1997**.
[54] G. M. Sheldrick, SHELXTL Reference Manual Version 5.1, Madison, WI, **1997**.

Received: August 19, 2005
Published online: January 13, 2006

